Energy Conversion and Management 271 (2022) 116312

Contents lists available at ScienceDirect

Energy Conversion and Management

journal homepage: www.elsevier.com/locate/enconman

Brayton technology for Concentrated Solar Power plants: Comparative analysis of central tower plants and parabolic dish farms

J. García-Ferrero, R.P. Merchán *, M.J. Santos, A. Medina, A. Calvo Hernández

Department of Applied Physics and IUFFYM, Universidad de Salamanca, Salamanca, Spain

ARTICLE INFO

Keywords:
Concentrated solar power
Central tower plants
Parabolic dish systems
Brayton cycles
Thermo-economic analysis
Local solar resources and ambient temperatures

ABSTRACT

Concentrated solar power plants intend to be key in the pool of renewable energy production technologies in the next future because of their versatility and high efficiency. In this work a comparative study between two promising technologies is developed. A central tower receiver surrounded by a heliostat field and a farm of parabolic dishes, both coupled to a hybrid Brayton cycle, are considered. Two power scales are surveyed (between 5 and 20 MW) at three different locations with quite different latitudes (between Sahara desert and medium European latitudes) and meteorological conditions. A modelling scheme developed by our group that allows to obtain the expected thermodynamic and thermo-economic plant records is applied. Key indicators like efficiency, net generated energy, levelized cost of electricity, and specific plant investment are calculated and analysed. Variability of natural gas prices and also land cost uncertainty are reflected on levelized cost of electricity range. Among the plants compared, minimum values are found within the interval [135–163] USD/MWh for central towers at the highest power considered and southern latitudes. In addition, the area needed for the installation of the plants and the influence of CO_2 taxes is also analysed. Displayed cashflows show larger investment costs for central tower than for dish farms. Finally, those systems are put into the context of other concentrated solar power, other renewable, like wind or photovoltaic, and other conventional power plants.

1. Introduction

Increasing energy demand together with fuel combustion concerns are the main drivers in the research of alternative and less polluting energy sources. A key advantage of Concentrated Solar Power (CSP) [1] plants over other renewable installations is the possibility of producing energy in a predictable and controllable way through hybridization [2] and/or storage [3]. Nowadays, most commercial CSP plants are a combination of Rankine cycles at medium temperatures together with Parabolic Trough collectors (PT) [4] or Central Tower receiver (CT) systems [5]. Nevertheless, larger efficiency layouts are being investigated through higher temperatures related to Brayton cycles [6]. On the way to fully functional plants with Thermal Energy Storage (TES), hybridization stands out as an intermediate step that allows reaching high temperatures in a straightforward way. However, this does not spoil that completely renewable plants, capable to produce energy fitting demand requirements, independently of seasonal or weather fluctuations, would be the final objective of this kind of studies [7]. With this aim, the development of high temperature and flexible storage systems will be required [8].

Recently, our group published an extensive analysis of the state-of-the-art and the expected research working lines for the next future on the field [9]. Briefly, some highlights are summarized here in order to bring to light the role of the investigation presented in this work. The working principle of CSP plants is quite simple, mirrors with different geometries reflect and concentrate direct solar radiation into a solar receiver. A working fluid flows through it reaching relatively high temperatures (approximately between 500 and 1000 °C). This fluid follows a thermodynamic cycle where heat input is transformed in mechanical work usually associated with the rotation of a turbine. Finally, an electrical subsystem transforms in turn this mechanical power in electrical power.

As these plants work with Direct Normal Irradiance (DNI), best locations are in principle those with higher DNI records. Usually regions between 15° and 40° at north or south latitudes are considered the best ones [2]. Nevertheless, sometimes another key ingredient to reach high efficiencies is forgotten, the mean ambient temperature at the plant site. In principle, locations with lower average temperatures are good to obtain high thermal efficiencies in the thermodynamic cycle that

* Corresponding author.
E-mail addresses: jgferrero@usal.es (J. García-Ferrero), rpmerchan@usal.es (R.P. Merchán), smjesus@usal.es (M.J. Santos), amd385@usal.es (A. Medina), anca@usal.es (A. Calvo Hernández).

https://doi.org/10.1016/j.enconman.2022.116312
Received 10 March 2022; Received in revised form 31 August 2022; Accepted 29 September 2022

Nomenclature

A_a	Aperture area of the field
A_r	Receiver area
C	Concentration factor
C_{dec}	Decommissioning costs
C_{inv}	Investment and initial installation costs
C_{OML}	Operation, maintenance and labour costs
$\cos\omega$	Cosine of Sun radiation angle of incidence
c_w	Specific heat of the working fluid
E_{net}	Net energy produced in a year
E_0	Net energy produced on the first operation year
f	Solar share
f_{at}	Attenuation factor
f_b	Blocking factor
f_{sh}	Shadowing factor
f_{sp}	Spillage factor
G	Direct normal irradiance
i	Real interest rate
k_{ins}	Annual plant insurance rate
$\dot{m}$	Mass flow of the working fluid
$\dot{m}_f$	Fuel mass flow rate
n_{con}	Number of years expended in plant construction
n_{dec}	Number of years expended in plant decommissioning
n_{op}	Number of years of plant operation
NH	Number of heliostats in the field
P	Power output
P_{nom}	Nominal power output
$\lvert\dot{Q}_{\text{H}}\rvert$	Total heat transfer rate absorbed by the working fluid
$\lvert\dot{Q}_{\text{HC}}\rvert$	Heat rate input from the combustion chamber
$\lvert\dot{Q}_{\text{HS}}\rvert$	Heat rate input from the solar collector
$\lvert\dot{Q}_{\text{L}}\rvert$	Heat-transfer rate between the working fluid and the ambient
Q_{LHV}	Lower heating value of the fuel
T_{HC}	Working temperature of the combustion chamber
T_{HS}	Working temperature of the solar collector
T_{L}	Ambient temperature
T_x	Working fluid temperature after the heat input from the recuperator
$T_{x'}$	Working fluid temperature after heat input from the solar collector
T_3	Turbine inlet temperature
$\overline{U}_{\text{L}}$	Effective conduction–convection heat transfer parameter

Greek symbols

α	Effective emissivity of the receiver
β_{dec}	Yearly equivalent cost of decommissioning factor
β_{DF}	DF factor
β_{inv}	Yearly equivalent capital investment cost factor
β_{OML}	OML factor
ε_{HC}	Combustion chamber heat exchanger effectiveness
ε_{HS}	Solar collector heat exchanger effectiveness
η	Overall thermal efficiency
η_C	Combustion chamber efficiency
η_{hel_i}	Efficiency of heliostat i
η_{H}	Thermal efficiency of the Brayton heat engine
η_S	Solar subsystem efficiency (field and receiver)
η_0	Heliostat field optical efficiency
ρ	Mirrors reflectivity
σ	Stefan–Boltzmann constant

Acronyms

ADGT	AeroDerivative Gas Turbines
BCR	Benefit to Cost Ratio
CCGT	Combined Cycle Gas Turbines
CRF	Capital Recovery Factor
CSP	Concentrated Solar Power
CT	Central Tower receiver
DF	Degradation Factor
DNI	Direct Normal Irradiance
DPP	Discounted Payback Period
IRR	Internal Rate of Return
LCoE	Levelized Cost of Electricity
MERRA	Modern-Era Retrospective Analysis for Research and Application
NPV	Net Present Value
OCGT	Open Cycle Gas Turbines
OML	Operation, Maintenance and Labour
PD	Parabolic Dish
PDF	Parabolic Dish Farm
PPA	Power Purchase Agreement
PT	Parabolic Trough collector
PV	Photovoltaic
SOLUGAS	Solar Up-scale Gas Turbine System
SPI	Specific Plant Investment
TES	Thermal Energy Storage
USD	US Dollar

runs the power unit of the plant. This aspect has not been sufficiently addressed in the literature and is one of the motivations of the present work.

Recent works as [10] highlight that next generations of these plants should work at temperatures above approximately 700 °C in order to obtain the efficiency that allows to reach commercial profitability. These temperatures can be obtained with high concentration ratio solar collectors as parabolic dishes and central towers. From the thermodynamic viewpoint, Brayton cycles are very interesting to operate at such temperature levels. These cycles can operate with gases as simply air [11] or with supercritical fluids as CO_2 in order to increase power unit efficiency. The latter is a very active and promising research line [12]. Another point that is deserving an extensive simulation and experimental work is the one related to optimize the design and materials of the solar receiver. This is a key element particularly for Brayton cycles that operate with gases or supercritical fluids. For instance, solar particle-based solar receivers are being investigated [13]. A comprehensive review about innovative solar receivers is due to Sedighi et al. [14].

Moreover, Brayton cycles for CSP plants can be hybridized in a straightforward way by using a combustion chamber [8] and also heat storage is also feasible, although more research along this line is necessary in the next years as suggested in a detailed review by Palacios and coworkers [7].

This work is focused on studying two different CSP collectors with similar power units, based on high temperature Brayton cycles working with air. The two CSP geometries are a Central Tower receiver

surrounded by a heliostat field and a Parabolic Dish Farm (PDF). A model that has already been previously developed for the power unit by this research group will be applied to such plant configurations. In [15] a complete model was presented for the whole plant including submodels to the estimation of the optical efficiency of an heliostat field surrounding a central tower and the thermal efficiency of the Brayton cycle. A design optimization and off-design analysis were presented in [16]. A thermo-economic study of a central tower plant hybridized with a combustion chamber burning natural gas was presented in [17]. A plant configuration with a solar dish connected to a micro gas turbine for distributed generation was developed in [18]. All these works contain the required models validations.

The mentioned models consider the coupling among several subsystems: solar collector, solar receiver, and power unit (including hybridization). Different heat exchangers are key in the coupling between subsystems. The Brayton power unit model in the present work is similar for CT and PDF. It is designed from a thermodynamic viewpoint and includes all irreversibility sources. The optical model for the heliostat field in the case of CT considers all the factors required to obtain precise estimations of the optical efficiency. For PDF plants, a single dish model is assumed, and the farm is considered as an additive array of dishes. All subsystem models and the coupling among them were validated in previous works. On-design and off-design simulations are feasible in the scheme developed and particularly seasonal or yearly averages are possible. In this work, real data for Direct Normal Irradiance (DNI) and ambient temperatures were considered, so annual estimations are accurate.

The methodology followed in this work consists in translating those optical and thermodynamic models to *Mathematica* programming language [19], in such a way that precise predictions for whichever plant location and climatological conditions can be obtained at on- and off-design conditions. With the goal of testing power scaling up impact, two power levels will be considered for each thermosolar geometry: 4.6 and 20 MW. Moreover, the influence of latitude on plant performance will be assessed via a location study. In this way, the comparison of the results at three sites with almost the same longitude, but with different latitudes, will illustrate that effect: one in Morocco (Ouarzazate) and two in Spain (Seville and Salamanca).

In a first section, concentration factor, solar share, net energy, efficiencies, fuel consumption, and CO_2 emissions are evaluated. Those main thermodynamic records are compared at three different levels: solar collector, power scale and location. The analyses would be incomplete without a bankability evaluation. Hence, key thermo-economic indicators as the Specific Plant Investment (SPI), the Levelized Cost of Electricity (LCoE), the Net Present Value (NPV), the Benefit to Cost Ratio (BCR), the Internal Rate of Return (IRR), and the Discounted Payback Period (DPP) are computed. Special attention is also paid to the land area that the plant requires. Similar to the case of the thermodynamic variables, plants are analysed at the same three aspects (geometry, scale and location). But, in this case, the comparison goes further by considering other CSP installations, other renewable and more conventional both real plants and studies. Regarding previous works presented by the authors as mentioned above, this study contains several improvements among which the whole thermo-economic study and the comparison both with other technologies and at the three already mentioned aspects are stressed. A key outcome is that other plant locations rather than the typical ones at low latitudes, but still with medium–high DNI records, could be considered for CT and PDF installations. This is because average ambient temperatures greatly affect overall plant thermal efficiency. Finally, the importance of a LCoE and SPI further reduction, and so a NPV increment, is highlighted.

2. Technology modelling

In this study two technological options for producing clean electricity running the same type of thermal power unit are considered. On one hand, a solar field reflecting direct solar radiation to a Central Tower receiver (CT) and, on the other hand, an array of solar Parabolic Dishes (PD). In both cases, the power unit that benefits from the solar heat generated in the solar subsystem runs a single-stage and recuperative Brayton cycle. For CT, there is only one gas turbine located at the tower top, behind the receiver, or in the basement besides the tower. For the solar dishes farm, each parabolic dish incorporates a micro-gas turbine located at the paraboloid focus. An illustrative scheme of both kinds of plants is depicted in Fig. 1.

2.1. Optical models and efficiencies of the solar subsystems

The aim of the solar subsystem is to provide heat to the power unit that develops the thermodynamic cycle. Direct solar radiation is reflected and concentrated to a solar receiver that is the key plant component because it has a dual function. It receives the concentrated solar power and transfers it to the working fluid that the power unit uses, *i.e.*, it acts somehow like a heat exchanger. Thus, the efficiency of the solar subsystems has two main components, the optical one, that measures the fraction of the incident radiation that is effectively collected in the receivers, and the one associated with the heat transfers from the receivers to their surroundings. In the following subsections, a summary of the main assumptions to calculate optical efficiencies for heliostat fields and solar dishes are presented.

2.1.1. Heliostat fields for central tower plants

For central tower plants, the solar collector is formed by an array of plane heliostats surrounding the central tower with an approximately circular symmetry or with a polar one (in the case of the Northern Hemisphere heliostats are concentrated at the north of the tower). In any case, heliostats have a two-axis tracking system in order to receive and reflect direct solar radiation in an efficient way towards the tower. Heliostats are distributed in the field in rows and regions and at least separated by a minimum security distance. There has been a large amount of research works during the last years about the optimum ways to distribute heliostats in the field [20,21]. In this work, circular and polar fields are considered. For both layouts, simulation codes were built from scratch in Mathematica [15,16]. Validation by comparison with recognized simulation packages was done in those papers. A brief summary is next presented, more details can be found in those references.

The procedure is based upon the methodology proposed by Collado [22,23]. The model develops an iterative process from an initially dense distribution of mirrors. Close mirrors distributions are capable to collect more solar power but shadowing and blocking effects decrease efficiency, thus there is an optimum number of heliostats (or distances among them) given an intended power range or surface area. The optical efficiency of each heliostat is calculated as:

$$\eta_{\mathrm{hel}_i} = \cos\,\omega_i \cdot f_{\mathrm{sp},i} \cdot f_{\mathrm{at},i} \cdot f_b \cdot f_{\mathrm{sh}} \cdot \rho \tag{1}$$

where $\cos\,\omega$ denotes the cosine of Sun radiation angle of incidence, f_{sp} comes from spillage, f_{at} is the attenuation factor, f_b represents the blocking factor, f_{sh} is the shadowing factor, and ρ represents mirrors reflectivity. A subindex i has been added in those terms that actually depend on each heliostat in this framework, others are considered as global average values.

The cosine factor is the key ingredient of optical efficiency. It is obtained from an analytical study of the geometry of the system Sun–heliostat–receiver and applying simple optical reflection laws; ω depends on each heliostat coordinates, receiver coordinates, and solar azimuth and altitude angles. The fraction of the radiation reflected by the mirrors that does not meet the receiver is called spillage, $f_{\mathrm{sp},i}$. It depends on the dimensions of the receiver, heliostat area, the effective dispersion of the sun shape on the receiver plane, heliostat tracking, and surface errors. Our codes assume the calculation model of the simulation tool HFLCAL [24] and a simplified version of that proposed

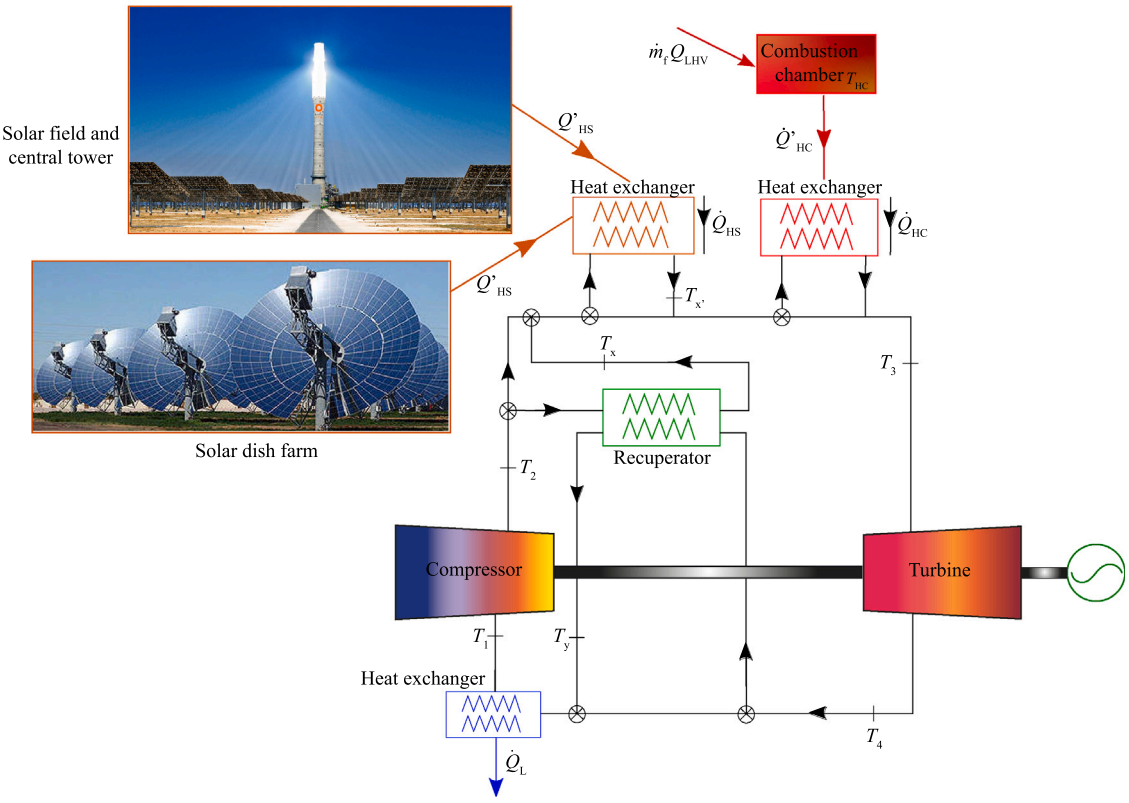

Fig. 1. Scheme of the two types of CSP systems considered: solar field and central tower system (CT) and solar parabolic dish farm (PDF). In both cases the power unit performs a single-stage recuperative hybrid Brayton cycle. State 1 represents compressor inlet conditions and state 3 turbine inlet conditions.

by Collado and Guallar in [25] (astigmatic effects are not considered). So, in this formulation the spillage factor depends on each heliostat position with respect to the receiver. The attenuation factor, $f_{\text{at},i}$, arises from the energy dissipation due to absorption of the atmospheric gases between the heliostats and the receiver. It depends on the particular distance between the centre of each heliostat and the aiming point in the receiver, and it is usual to take an empirical formula for $f_{\text{at},i}$ in terms of the distance [26]. The blocking factor measures the energy loss because a fraction of the reflected energy from a back heliostat can be stopped by one frontwards. The shadowing factor accounts for the energy loss when a heliostat projects a shadow onto another one. These factors, f_b and f_{sh}, are the most expensive from the computational viewpoint if calculated for each heliostat. Nevertheless, as the objective of this work concerns the overall plant, they will be taken as constant factors. This avoids too extensive computations and does not affect the reliability of the results for the plant [17,27]. Finally, mirrors reflectivity, ρ, is usually assumed as a constant factor depending on nominal mirrors reflectivity and cleanliness (thus, somehow it is related to plant maintenance costs).

The optical efficiency of the field, η_0, is given by the average of each heliostat efficiency, η_{hel_i}:

$$\eta_0 = \frac{\sum_{i=1}^{NH} \eta_{hel_i}}{NH} \tag{2}$$

where NH is the total number of heliostats in the field.

The validation of this submodel for circular [15] and polar fields [16] was previously published.

2.1.2. Parabolic dishes

In the case the plant is constituted by an array of solar dishes, each collector has a paraboloid shape with defined aperture diameter and focal distance. Direct solar radiation is collected to the receiver. Its diameter is a function of the concentration factor, $C = A_a/A_r$, where A_a is the irradiated aperture area of the dish and A_r is the receiver area. In this work, identical optical efficiency, η_0, for all dishes will be assumed. It is taken as a design parameter depending on dishes shape, reflective coatings and cleanliness, and particularities of the receiver [18]. An analysis of the validation of such assumptions was done in the same paper by performing independent simulations with the software Tonatiuth [28].

For both types of plants, heat transfer losses from the receiver to its surroundings is calculated in a simplified way, considering conduction, convection and radiation losses components [11,29]. Thus, the solar subsystem efficiency in both layouts is calculated as:

$$\eta_S = \eta_0 - \frac{1}{GC}[\alpha\sigma(T_{HS}^4 - T_L^4) + \overline{U}_L(T_{HS} - T_L)] \tag{3}$$

where G is the direct normal irradiance, α is the emissivity of the receiver surface, σ the Stefan–Boltzmann constant, and $\overline{U}_L$ the overall conduction and convection heat transfer coefficient. T_{HS} represents the solar receiver operation temperature and T_L the ambient temperature. T_{HS} is obtained by balancing the heat input in the receiver associated with solar radiation and the heat extracted by the working fluid, that in turn is the heat input in the thermodynamic cycle developed by the Brayton power unit.

2.2. Thermodynamic model for the power units

A Brayton-like cycle is assumed for the power units in both types of plants. Particularly, a simple (mono-stage) recuperative closed air Brayton cycle. The engine admits two types of heat input. One from the receiver, $\dot{Q}_{\text{HS}}$, when solar conditions are good and direct normal irradiance is above certain minimum value and another one from a combustion chamber burning natural gas for periods of bad solar resources or by night, $\dot{Q}_{\text{HC}}$. A schematic diagram of the $T-S$ cycle developed is depicted in Fig. 2.

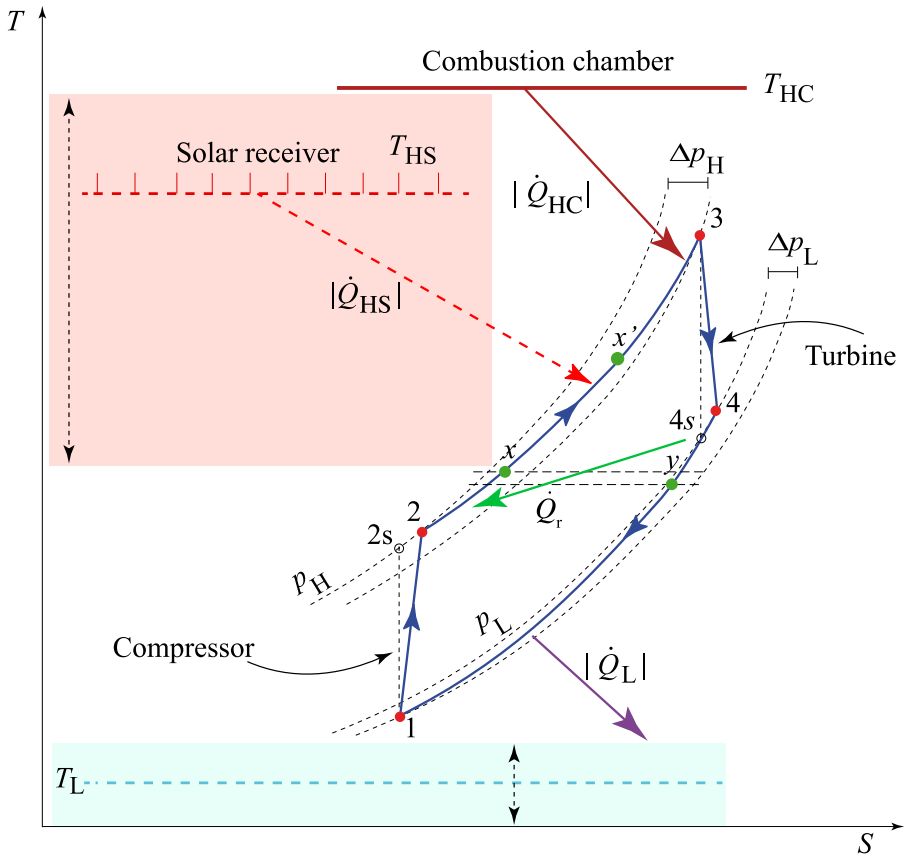

Fig. 2. Brayton-like cycle assumed for the power units. The temperatures T_{HS} and T_L fluctuate with solar radiation and meteorological conditions.

The thermal efficiency of the micro-gas turbine, η_h, is calculated from a theoretical development assuming a closed irreversible Brayton cycle with non-isentropic compressor and turbine, pressure losses in heat absorption and heat release processes, and a non-ideal recuperator. Losses are moreover considered in the heat input from the solar receiver and from the combustion chamber, and also in the heat release to the surroundings since they constitute the most significant losses in real gas turbines.

As shown in Fig. 2, the working gas is compressed from state 1 (compressor inlet) to state 2 in a non-isentropic compressor. Then, temperature increases up to T_x due to the recuperator connected to the turbine exit. During sunlight hours, if direct normal irradiance is enough, the receiver releases heat to increase the temperature up to $T_{x'}$. Turbine inlet temperature, T_3, is assumed as a fixed input parameter. If heat input in the solar receiver is not enough to reach that temperature, a combustion chamber burns natural gas to save the temperature difference. Pressure losses are considered in the receiver and in the heat input through the combustion chamber. After state 3, the fluid is expanded in the non-ideal turbine. Finally, the cycle is closed by means of a heat transfer to the recuperator and to the ambient through a heat exchanger. All the temperatures in the cycle can be obtained as analytical expressions in terms of the compressor pressure ratio and parameters quantifying the considered irreversibilities. Explicit equations can be found in [15]. The model has been previously detailed and validated for central tower plants [11] and also for solar dishes [18]. It was developed in order to be comprehensive and analytical to make possible sensitivity and optimization analyses. Validation showed that their results compare favourably with those of standard open cycle gas turbines [30].

The heat engine efficiency is defined as $\eta_h = P/|\dot{Q}_H|$, where $|\dot{Q}_H|$ is the total heat input rate, $|\dot{Q}_H| = |\dot{Q}_{HS}| + |\dot{Q}_{HC}|$ and P is the output power $P = |\dot{Q}_H| - |\dot{Q}_L|$, where $|\dot{Q}_L|$ is the heat release to the surroundings. The ratio between the solar heat input and the total one is the solar share, $f = |\dot{Q}_{HS}|/|\dot{Q}_H|$.

$$|\dot{Q}_{HS}| = \dot{m} \int_{T_x}^{T_{x'}} c_w(T)\, dT = f|\dot{Q}_H| \tag{4}$$

$$|\dot{Q}_{HC}| = \dot{m} \int_{T_{x'}}^{T_3} c_w(T)\, dT = (1-f)|\dot{Q}_H| \tag{5}$$

where $\dot{m}$ is the mass flow of the working fluid, which is air in this study. The heat release to the surroundings is expressed as:

$$|\dot{Q}_L| = \dot{m} \int_{T_1}^{T_y} c_w(T)\, dT \tag{6}$$

In these equations, $c_w(T)$ represents the temperature dependent constant pressure specific heat of the working fluid. Explicit calculations of all these heat flows can be found in [11].

The efficiency of the combustion chamber, η_c, is taken as a constant parameter. In real installations it could slightly change with fluctuations of the fuel–air equivalence ratio, the composition of the fuel, its temperature, and several other variables, but the realistic interval of possible values for η_c is quite narrow. The heat received by the working fluid from the combustion chamber, $\dot{Q}_{HC}$, can be written as:

$$|\dot{Q}_{HC}| = \varepsilon_{HC}|\dot{Q}'_{HC}| = \varepsilon_{HC}\, \eta_C\, \dot{m}_f\, Q_{LHV} \tag{7}$$

where Q_{LHV} is the lower heating value of the fuel and $\dot{m}_f$ is the fuel mass flow entering in the combustion chamber at any time instant. ε_{HC} is the effectiveness of the heat exchanger in between the combustion chamber and the thermal cycle. As fluctuations in G and T_L are explicitly considered, the fuel mass flow to be burned in the combustion chamber will also be a time dependent function given by:

$$\dot{m}_f = \frac{|\dot{Q}_{HC}|}{\eta_C\, Q_{LHV}\, \varepsilon_{HC}} \tag{8}$$

where $|\dot{Q}_{HC}|$ is obtained from Eq. (5).

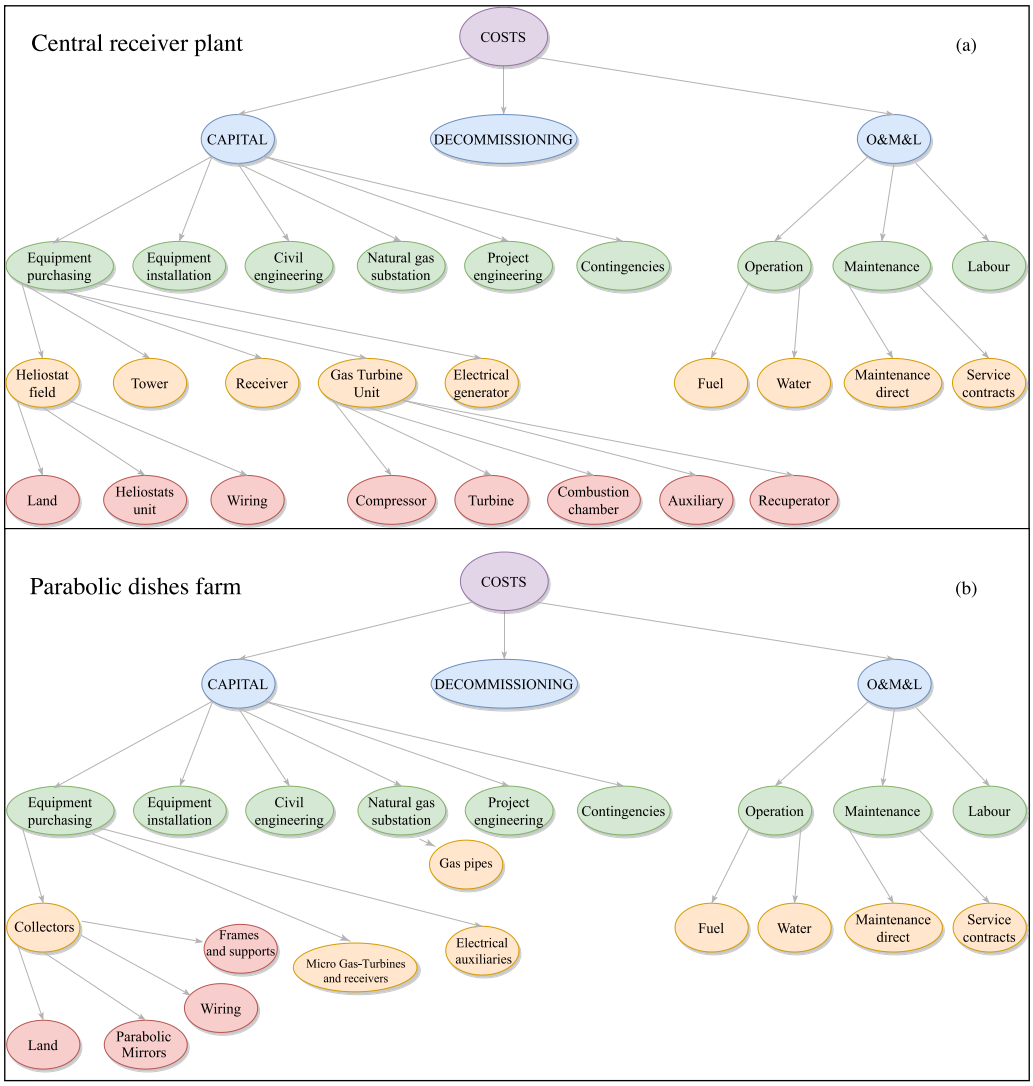

Fig. 3. Scheme of the components considered for the calculation of LCoE values and other economic indicators: (a) Central tower plants and (b) solar dishes farm.

This submodel for the Brayton power cycle was validated in several previous papers, for instance: in [30] by comparing model predictions with a commercial 4.6 MW gas turbine, in [15] comparing with a 20 MW gas turbine and in [18] by comparing against a 30 kWe micro gas turbine.

2.3. Overall plant thermal efficiency

The ratio between the net power output and the total energy input per unit time is the overall plant thermal efficiency, η:

$$\eta = \frac{P}{G A_a + \dot{m}_f Q_{\mathrm{LHV}}} \tag{9}$$

where A_a is the aperture area. Overall efficiency, η, can be expressed as a combination of the efficiencies of the subsystems (η_s, solar collector and receiver; η_c, combustion chamber; and η_h, heat engine efficiencies), the solar share, f (fraction of the total heat input due to sun irradiance), and the effectiveness of the heat exchanges from the receiver and the combustion chamber to the fluid (ε_{HS} and ε_{HC}, respectively):

$$\eta = \eta_s \eta_c \eta_h \left[\frac{\varepsilon_{HS}\varepsilon_{HC}}{\eta_c f \varepsilon_{HC} + \eta_s (1-f)\varepsilon_{HS}} \right]. \tag{10}$$

Explicit calculations to obtain this equation can be found in [11,31]. When the only heat input comes from the solar receiver (good solar conditions) $f = 1$ and $\eta = \eta_s \eta_h \varepsilon_{HS}$ and in the only combustion mode (by night or bad solar conditions) $f = 0$ and $\eta = \eta_c \eta_h \varepsilon_{HC}$.

2.4. Thermo-economic indicators for CSP plants

In these subsections, the definitions of the main indicators elected to survey the thermo-economic profile of the considered plant configurations are briefly presented.

2.4.1. Levelized cost of electricity (LCoE)

LCoE represents the minimum price at which electricity should be sold for the plant to be cost-effective or profitable. It is defined as:

$$\mathrm{LCoE} = \frac{\beta_{\mathrm{inv}} \cdot C_{\mathrm{inv}} + \beta_{\mathrm{dec}} \cdot C_{\mathrm{dec}} + \beta_{\mathrm{OML}} \cdot C_{\mathrm{OML}}}{E_0} \beta_{\mathrm{DF}} \tag{11}$$

Numerator and denominator are given in annual terms:

- C_{inv} represents the total investment and initial installation costs.
- C_{dec} is the total decommissioning costs.
- The weight β_{inv} relates the total capital investment costs to the equivalent annual payments over a fixed period of years. Similarly, β_{dec} represents the yearly equivalent cost of decommissioning. These factors can be written as [32]:

$$\beta_{\mathrm{inv}} = \frac{(1+i)^{n_{\mathrm{op}}}[(1+i)^{n_{\mathrm{con}}} - 1]}{n_{\mathrm{con}}} + k_{\mathrm{ins}}[(1+i)^{n_{\mathrm{op}}} - 1] \tag{12}$$

$$\beta_{\mathrm{dec}} = \frac{1 - (1+i)^{-n_{\mathrm{dec}}}}{n_{\mathrm{dec}}} \tag{13}$$

$$\beta_{\mathrm{OML}} = (1+i)^{n_{\mathrm{op}}} - 1 \tag{14}$$

$$\beta_{\mathrm{DF}} = \frac{(\mathrm{DF}+i)}{i[(1+i)^{n_{\mathrm{op}}} - (1-\mathrm{DF})^{n_{\mathrm{op}}}]} \tag{15}$$

- C_{OML} corresponds to the annual operation, maintenance and labour costs (OML), which include fuel consumption in the case of hybrid plants
- E_0 stands for the net energy output on the first operation year.

In these equations, i is the real interest rate (or discount rate) and k_{ins} is the annual plant insurance rate. The number of years expended in plant construction, operation, and decommissioning are denoted n_{con}, n_{op}, and n_{dec}, respectively. The term $\frac{i\cdot(1+i)^{n_{op}}}{(1+i)^{n_{op}}-1}$ is called capital recovery factor (CRF). If there are losses in the annual net energy associated with plant degradation [33], they are incorporated in the degradation factor, DF. In that case, annual energy decreases with time as:

$$E_{\mathrm{t}'} = E_0(1-\mathrm{DF})^{\mathrm{t}'} \tag{16}$$

$$\mathrm{t}' = \mathrm{t} - n_{\mathrm{con}} \tag{17}$$

As shown in the equations, this formulation of LCoE explicitly considers the time spent during construction and decommissioning. In other formulations these times are considered as one year, but in this case these times could be longer. Fig. 3 depicts all the terms considered for LCoE computation in the case of central receiver and of a farm of parabolic dishes. In both cases, the power unit is considered as a hybrid gas turbine engine.

2.4.2. Net present value (NPV)

NPV is another measure of project profitability: a positive value indicates that project is feasible while a negative one indicates that the project is economically unfeasible. It is the sum over the operation years of the net cash flows (annual revenues of selling electricity less annual operation and maintenance costs) less the total investment and decomissioning costs.

$$\mathrm{NPV} = -\sum_{t=0}^{n_{\mathrm{con}}-1}\frac{C_{\mathrm{inv}}}{n_{\mathrm{con}}(1+i)^t} + \sum_{t=n_{\mathrm{con}}}^{n_{\mathrm{con}}+n_{\mathrm{op}}-1}\frac{E_{\mathrm{t}'}\cdot\mathrm{PPA} - (C_{\mathrm{OML}}+C_{\mathrm{ins}})}{(1+i)^t} - \sum_{t=n_{\mathrm{con}}+n_{\mathrm{op}}}^{n_{\mathrm{con}}+n_{\mathrm{op}}+n_{\mathrm{dec}}-1}\frac{C_{\mathrm{dec}}}{n_{\mathrm{dec}}(1+i)^t} \tag{18}$$

where PPA is the Power Purchase Agreement, a deal between electricity seller and purchaser. Most developed countries have guaranteed PPA tariffs for renewable energy plants (in the case of renewable technologies it is usually called *feed-in tariff*). In the case NPV = 0, then PPA = LCoE.

2.4.3. Benefit to cost ratio (BCR)

It is defined as the ratio between the total profit and the total investment cost, defined in such a way that BCR > 1 indicates a profitable plant and BCR < 1 a non-viable one.

$$\mathrm{BCR} = 1 + \frac{\mathrm{NPV}}{C_{\mathrm{inv}}} \tag{19}$$

2.4.4. Specific plant investment (SPI)

It is defined as the total investment required to build a plant with respect to its nominal power output, expressed in €/kWe or $/kWe:

$$\mathrm{SPI} = \frac{C_{\mathrm{inv}}}{P_{\mathrm{nom}}} \tag{20}$$

2.4.5. Internal rate of return (IRR)

It is the annual rate of growth an investment is expected to generate. The higher IRR, the more desirable an investment is to undertake. It represents a way to estimate which is the rate of interest the initial investment is predicted to produce.

$$\mathrm{NPV} = -\sum_{t=0}^{n_{\mathrm{con}}-1}\frac{C_{\mathrm{inv}}}{n_{\mathrm{con}}(1+IRR)^t} + \sum_{t=n_{\mathrm{con}}}^{n_{\mathrm{con}}+n_{\mathrm{op}}-1}\frac{E_{\mathrm{t}'}\cdot\mathrm{PPA} - (C_{\mathrm{OML}}+C_{\mathrm{ins}})}{(1+IRR)^t} - \sum_{t=n_{\mathrm{con}}+n_{\mathrm{op}}}^{n_{\mathrm{con}}+n_{\mathrm{op}}+n_{\mathrm{dec}}-1}\frac{C_{\mathrm{dec}}}{n_{\mathrm{dec}}(1+IRR)^t} = 0 \tag{21}$$

2.4.6. Discounted payback period (DPP)

It represents the time required to recover the initial investment considering interest rates [36], *i.e.*, the number of operation years that make NPV positive:

$$\mathrm{NPV} = -\sum_{t=0}^{n_{\mathrm{con}}-1}\frac{C_{\mathrm{inv}}}{n_{\mathrm{con}}(1+i)^t} + \sum_{t=n_{\mathrm{con}}}^{n_{\mathrm{con}}+\mathrm{DPP}-1}\frac{E_{\mathrm{t}'}\cdot\mathrm{PPA} - (C_{\mathrm{OML}}+C_{\mathrm{ins}})}{(1+i)^t} - \sum_{t=n_{\mathrm{con}}+\mathrm{DPP}}^{n_{\mathrm{con}}+\mathrm{DPP}+n_{\mathrm{dec}}-1}\frac{C_{\mathrm{dec}}}{n_{\mathrm{dec}}(1+i)^t} > 0 \tag{22}$$

3. Numerical data and design points

This study is focused on analysing the performance (thermal and thermo-economic) of the same type of power unit (simple Brayton-like cycle) connected to two different CSP technologies (central tower and solar dish farm) at different locations (from the Sahara desert to northern latitudes in Europe). This section compiles all the data required to perform the computational calculations: meteorological, solar subsystems and Brayton power unit, and input data required for thermo-economic estimations.

3.1. Locations and meteorological data

Three locations at approximately the same longitude but different latitudes in the Northern hemisphere have been chosen (see Fig. 4). Moreover, their climatological conditions are quite different. Real data for ambient temperature, T_L, and direct normal irradiance, G, were taken to perform calculations. Ambient temperatures were taken from MERRA [44] (*Modern-Era Retrospective Analysis for Research and Applications*) and G from *Copernicus, Europe's Eyes on Earth* [34].

Next, the peculiarities of the three selected locations are summarized from south to north. Ouarzazate at Morocco (30.92°N latitude) is, in principle, a suitable location for CSP installations because of its large solar resources. Annual direct normal irradiation is over 2500 kWh/m^2 and averaged peak G value is about 800 W/m^2. Mean minimum temperature is around 282 K and maximum around 294 K. Seville (Spain) (37.44°N latitude) is located approximately 750 kms to the north of Ouarzazate. Averaged annual direct irradiance is around 1975 kWh/m^2 (21% below Ouarzazate). Average temperatures are above Ouarzazate, about 3 K above both minimum and maximum temperatures and mean maximum value of G is slightly below 700 W/m^2. Seville is also (as Ouarzazate) a typical location for CSP plants. Salamanca (450 km to the north of Seville, 40.98°N latitude), has a priori worse annual direct normal irradiation, about 1834 kWh/m^2 (26.7% below Ouarzazate) and also lower G peaks (the annual mean is about 500 W/m^2). Yearly averaged mean temperatures are below Ouarzazate and Seville. For instance, comparing with Seville mean minimum temperature is 5 K below and mean maximum daily temperature is 7 K below. This is because climate is continental and also because Salamanca is atop a plateau about 800 m above sea level and daily oscillations of temperature are large. Up-to-date Salamanca has not been considered for CSP plants establishment.

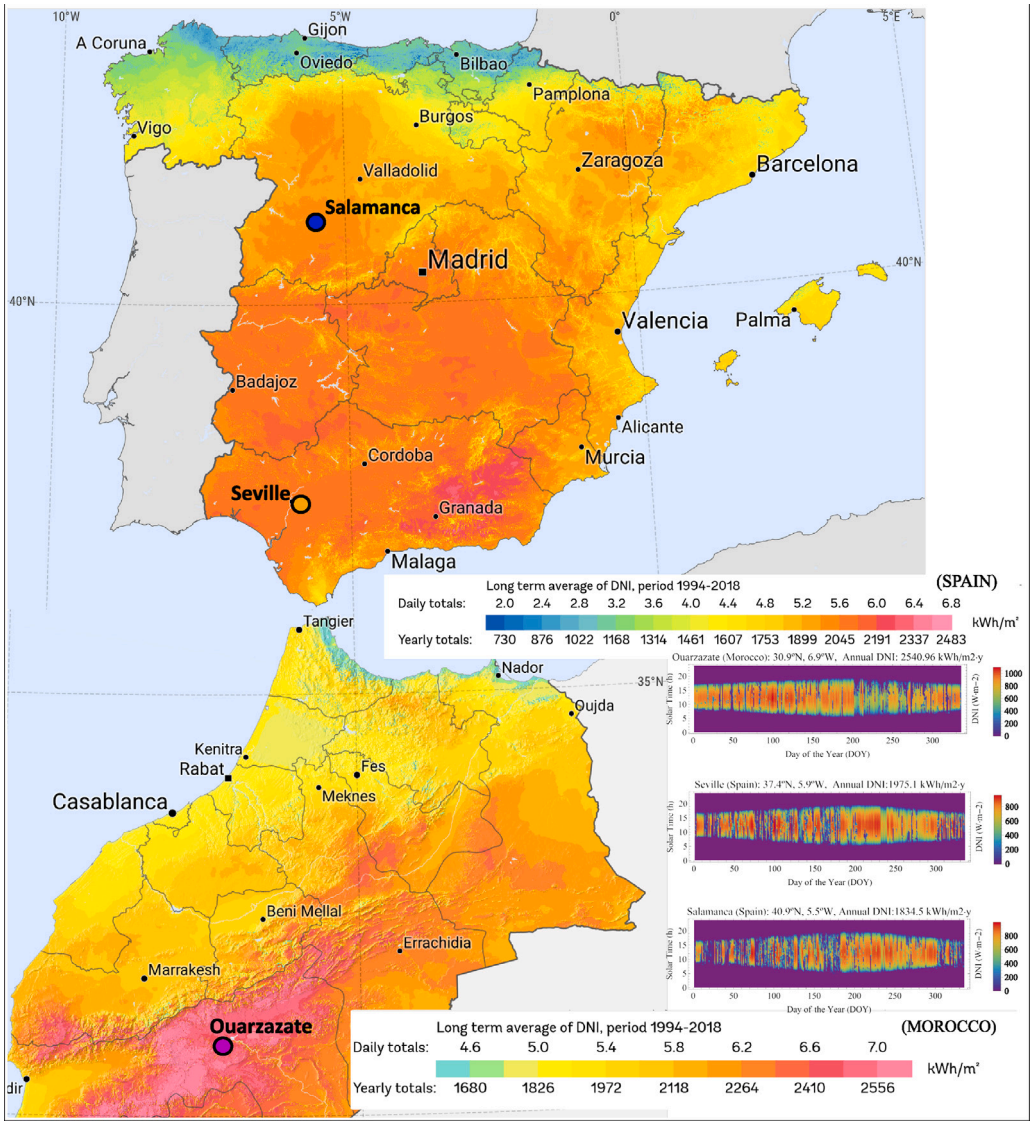

Fig. 4. Locations considered for the analysis and annual direct irradiation data (bottom right). Direct irradiation oscillations data correspond to 2018 [34]. *Source:* Map adapted from SOLARGIS [35].

3.2. Solar subsystems and power unit input data

The computational model was applied to the three mentioned locations at two power levels, 4.6 and 20 MW. Tables 1 and 2 summarize the required input parameters, including all plant subsystems: solar subsystem, combustion chamber for hybridization, and Brayton power units. In the case of central tower plants, the projects SOLUGAS (polar field and 4.6 MW of power output approximately) [37] and GEMASOLAR (polar field and 20 MW of power output approximately) [38] were taken as references, and real gas turbines were considered [39,40]. Some parameters as heliostats number, concentration ratio, and solar thermal power slightly depend on the selected location because of heliostat field design. More details on the numerical implementation of the model for central towers can be found at [15,17].

Table 2 compiles the data required to simulate the solar dish farms. For both power levels, dishes were considered identical (with an aperture area of 169.4 m^2) and the number of dishes is 200 for a power output of 4.6 MW and 870 for 20 MW. In this case, it is considered that each receiver at the dish focus incorporates a micro-gas turbine with the parameters given in the table. Most parameters were taken from the works of Semprini et al. [41] and Giostri et al. [43].

3.3. Input data for thermo-economic estimations

Tables 3–5 summarizes the data used to perform the thermo-economic estimations. Data were taken from [32]. Construction, operation, and decommissioning periods are taken identical for both types of plants as shown in Table 3.

Table 4 displays the costs calculated for the computation of LCoE and other economic indicators in the case of central tower systems. Particularly, the data in the table corresponds to Seville and were mainly taken from Refs. [32,52–54]. As it will be shown in the results section, natural gas costs were considered in a wide interval, from 18.39 to 29.71 USD/MWh [55]. These are reference prices in Spain. In particular, in Tables 4 and 5, the cheapest prices in the interval are shown. In subsequent sections, the importance of natural gas price fluctuations will be analysed. Land and water costs were also assumed as reference values for Spain with the aim of a straightforward comparison. In general, water cost was taken as 1.72 USD/m^3 [56] and land cost 6748.2 USD/ha [57], except for LCoE interval computation. In that case, the most expensive LCoE is calculated with the most expensive natural gas price (29.71 USD/MWh), but also with an expensive land cost (22490.39 USD/ha). Nevertheless, for the lower limit, the cheapest natural gas (18.39 USD/MWh) and land (6748.2 USD/ha) costs are

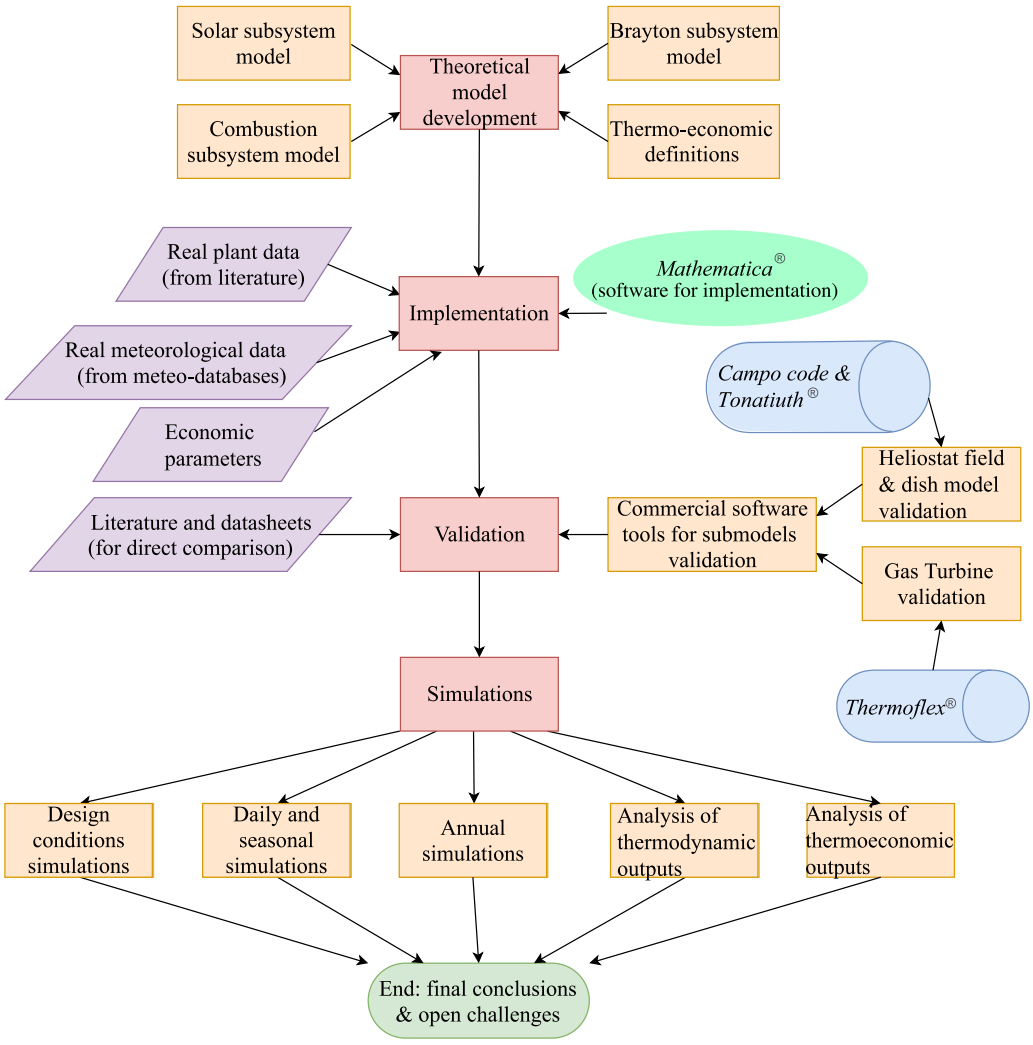

Fig. 5. Flow chart diagram of the work development. Cylinders refer to external standard software used for validation purposes and rhomboids to the different types of data required to run simulations. Programming software used to build the simulations is *Mathematica*.

considered. In the case of the solar dish array, Table 5, data were taken from Refs. [32,54,58,59].

3.4. Simulations structure and implementation

A flow diagram of the way submodels are implemented and simulations are structured is depicted in Fig. 5. All subsystem submodels were implemented in Mathematica and independently validated, either by comparing with real data or by using commercial software. No commercial software was used to obtain thermodynamic of thermoeconomic results, it was only used for validation purposes. Thus, all the physical ingredients in this kind of plants and simplifying hypotheses are directly considered in the development of the framework.

As explained in the subsections before, three kinds of data were considered: from meteorological databases at the particular locations, from real plants for basic parameters (solar collectors, solar receivers and gas turbines dimensions), and economic parameters for thermoeconomic estimations. To obtain annual yields, daily and seasonal averages were performed before calculating yearly means.

4. Thermodynamic estimations

In this study, several thermodynamic variables are calculated and analysed in an annual basis like solar share, net energy, overall, heat engine, optical, and solar efficiencies, or specific fuel consumption and CO_2 emissions. Those output variables, obtained within the framework previously outlined, are gathered at Table 6 together with the corresponding concentration factors.

Analysed variables for parabolic dish farms are independent of power scale, as expected, because farms are considered as an additive array of dishes, so all extensive variables are additive. The only exception is annual generated energy. Concentration factors of dish farms are around 4–5 times higher than that of central towers. For PDs, the concentration factor does not depend on location nor power scale since the same parabolic dish unit is considered in all cases. Variations for CTs are not large. For the smallest power scale, a higher concentration factor is always achieved because of the particular solar field characteristics. Differences among locations are due to the adaptation of the field to the particular sites since solar receivers are assumed the same for all locations.

With respect to the solar share, a clear pattern is observed for all locations. The highest values are related to PDs, then CT at 20 MW and finally CT with 4.6 MW presents the lowest values. Better solar irradiation conditions are reflected into larger solar share. Hence, Ouarzazate presents the best values while Salamanca the lowest ones. The small solar share of CTs at 4.6 MW indicates that the solar field size is not enough for the desired gas turbine power, which is a consequence of the original design of SOLUGAS Project [17]. Their design characteristics were assumed in this work.

Table 1
Summary of key plant parameters. Data for 4.6 MW plant are based on SOLUGAS project [37] and 20 MW ones on GEMASOLAR plant [38]. The data in brackets corresponds to each location: [Ouarzazate, Seville, Salamanca]. The gas turbine for the SOLUGAS power output is a *Mercury 50* by Solar Turbines, Caterpillar [39] and in the case of GEMASOLAR the turbine is *Solar Titan 250*, also by Solar Turbines, Caterpillar [40]. More details and validation in Refs. [15,17].

Heliostat Field and Central Tower (CT)				
Subsystem	Parameter	4.6 MW	20 MW	Unit
Heliostat field and receiver	Tower height	65	150	m
	Heliostats number	[66, 69, 71]	[780, 873, 784]	–
	Heliostat height	11.01	10.95	m
	Heliostat area	121.3	120	m^2
	Adjacent heliostats separation	3.303	3.285	m
	Heliostat field minimum radius	64	65	m
	Concentration ratio	[408, 426, 439]	[338, 378, 340]	–
	Blocking and shadowing factor	0.95		–
	Actual mirrors reflectivity	0.836		–
	Sun shape deviation	2.51		mrad
	Surface errors deviation	0.94		mrad
	Tracking errors deviation	0.63		mrad
	Receiver diameter	5	8.4	m
	Receiver height	–	10.5	m
	Receiver emissivity	0.1		–
	Conduction and convection losses factor	5		$W/(m^2K)$
	Receiver (heat exchanger) effectiveness	0.78		–
	Solar thermal power	[5.30, 5.23, 5.28]	[62.14, 63.76, 55.84]	MW
Combustion system	Combustion chamber efficiency	0.98		–
	Heat exchanger efficiency	0.98		–
Brayton cycle	Pressure ratio	9.9	23.4	–
	Air mass flow	17.9	67	kg/s
	Turbine isentropic efficiency	0.885	0.92	–
	Compressor isentropic efficiency	0.815	0.895	–
	Turbine inlet temperature	1423	1451	K
	Recuperator effectiveness	0.775		–
	Ambient heat exchanger effectiveness	0.985		–
	Heat input pressure drop	9.4		%
	Heat release pressure drop	9.4		%
	Generator efficiency	0.98		–

Table 2
Plant data are mainly based on the work by Semprini et al. [41]. The data of the Brayton cycle correspond to the micro-gas turbine *Capstone C30* by Capstone Turbine Corporation [42].

Parabolic Dish Farm (PDF)				
Subsystem	Parameter	4.6 MW	20 MW	Unit
Parabolic dish field and receiver	Parabolic dishes number	200	870	–
	Collector aperture area (per unit)	169.40		m^2
	Adjacent parabolic dishes separation[a]	4.43		m
	Concentration ratio	1781		–
	Optical efficiency	0.9087		–
	Receiver diameter	0.3480		m
	Receiver emissivity	0.1		–
	Conduction and convection losses factor	5		$W/(m^2K)$
	Receiver effectiveness	0.7937		–
	Power output per unit	0.023		MWe
Combustion system	Combustion chamber efficiency	0.97		–
	Heat exchanger efficiency	0.97		–
Brayton cycle	Pressure ratio	3.75		–
	Air mass flow	0.2762		kg/s
	Turbine isentropic efficiency	0.76		–
	Compressor isentropic efficiency	0.76		–
	Turbine inlet temperature	1173.15		K
	Recuperator effectiveness	0.85		–
	Ambient heat exchanger effectiveness	1		–
	Heat input pressure drop	12.5		%
	Heat release pressure drop	0		%
	Generator and Power Control System (PCS) efficiency[b]	0.96		–
	Organic efficiency (shaft power/turbine rotor power)[b]	0.98		–

[a]Adapted from Abdelhady et al. [33]
[b]Taken from Giostri et al. [43]

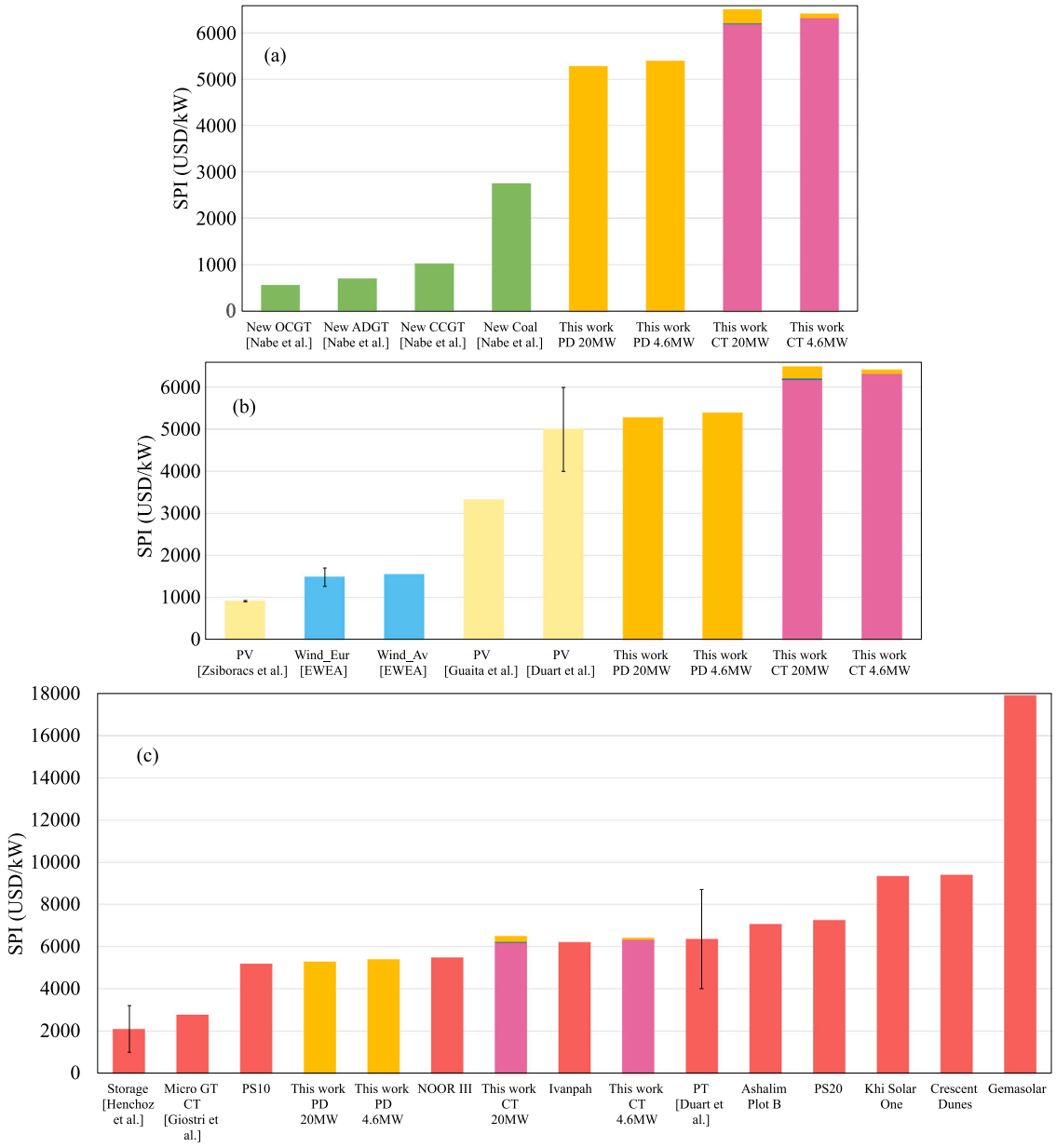

Fig. 6. Specific Plant Investment (SPI) in the context of other type of power facilities and system simulations: (a) conventional plants, (b) other renewable installations and (c) CSP projects. Magenta, orange and blue bars are associated with simulations at Ouarzazate, Seville and Salamanca locations, respectively. Cyan bars refer to wind energy, yellow ones to photovoltaic installations (PV), red ones to other CSP systems and green bars correspond to other power facilities values found in literature. OCGT refers to Open Cycle Gas Turbines, ADGT to AeroDerivative Gas Turbines, CCGT to Combined Cycle Gas Turbine and PT to Parabolic Troughs [45–51].

Table 3
Interest and time parameters assumed for the calculation of LCoE in both plants [32].

Parameter	Symbol	Value	Unit
Real interest rate	i	7	(%)
Annual plant insurance rate	k_{ins}	1	(%)
Construction time	n_{con}	2	year
Operation time	n_{op}	25	year
Decommissioning time	n_{dec}	2	year

Regarding net energy, small deviations are shown within each power scale. Nevertheless, a net energy of around 40 GWh/year is achieved for the 4.6 MW system and of about 180 GWh/year for the 20 MW power facility. For the PD system, higher energy records are related to Salamanca, the same that happens in the case of CTs when Salamanca plant generates a bigger amount of net energy. This fact will be explained below in terms of efficiencies.

Looking at the efficiencies, the lowest ambient temperature recorded in Salamanca boosts the heat engine efficiency, which is reflected on the overall thermal efficiency (see Table 6). Optical efficiencies in the case of central towers are very similar for each power level (around 0.65 for 4.6 MW and between 0.61 and 0.62 for 20 MW) although heliostat field geometries are not exactly the same (see Table 1). Having in mind the latter, no significant differences are found among different locations. As the same parabolic dish unit is assumed in all simulations, a constant optical efficiency of 0.909 is obtained for PD farms. Higher losses accounted in solar fields imply a lower optical efficiency for CTs. A small solar field (4.6 MW) has demonstrated to be more efficient than a higher one (20 MW). This behaviour determines solar subsystem efficiency (that compiles optical collector efficiencies and receiver efficiency, see Eq. (3)), which is still significantly higher for dish farms and which depends also on solar receiver losses. In this way, 20 MW CT system presents the lowest solar efficiency. Among

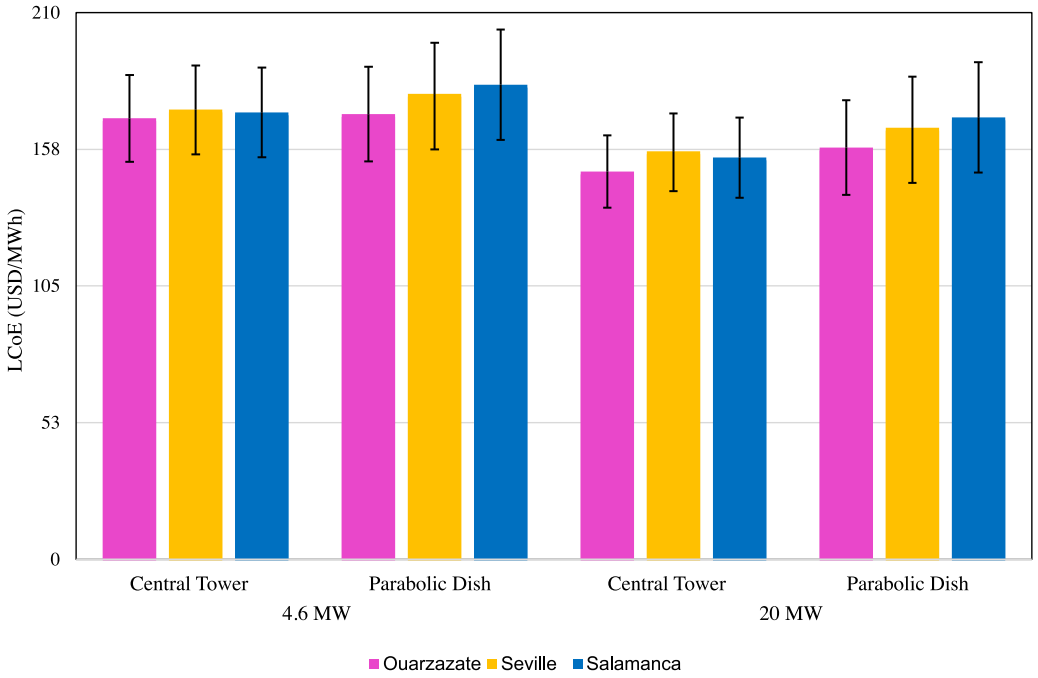

Fig. 7. Levelized Cost of Electricity (LCoE) for the three locations, two geometries and two power scales. Magenta bars are associated with simulations for Ouarzazate, orange ones with Seville and blue ones with Salamanca. Uncertainty bars correspond to fluctuations in natural gas and land prices.

Table 4
Costs calculated for the computation of LCoE at Seville location. All costs are expressed in Million USD except those from OML that are accounted in yearly terms, Million USD/year.
Source: All data were taken from [32,52–54].

Central Tower (CT)				
			4.6 MW	20 MW
			Cost (Million USD)	
Capital costs			29.36	141.32
Equipment purchasing			20.15	99.15
	Gas turbine unit		1.841	12.73
		Compressor	0.834	9.156
		Turbine	0.227	1.161
		Combustion chamber	5.085×10^{-3}	0.013
		Auxiliary	0.650	1.929
		Recuperator	0.124	0.470
	Heliostat field		5.938	46.88
		Land	0.509	1.983
		Heliostat units	5.375	44.12
		Wiring	0.05	0.771
	Tower		3.882	8.561
	Receiver		5.844	23.66
	Electrical generator		2.648	7.315
Equipment installation			4.031	19.83
Civil engineering			1.054	3.604
Natural gas substation			0.291	0.307
Project engineering			1.276	6.144
Contingencies			2.553	12.29
Decommissioning			1.276	6.144
			Cost (Million USD/year)	
Operation, maintenance and labour			2.989	10.91
Operation			1.811	7.174
	Fuel		1.810	7.165
	Water		7.832×10^{-4}	9.102×10^{-3}
Maintenance			0.601	2.867
	Direct maintenance		0.488	2.689
	Service contracts		0.113	0.178
Labour			0.577	0.866

analysed locations, Ouarzazate achieves the highest solar efficiency, η_S, with values up to 0.883 in dish farms.

Hence, the combination of all these behaviours results in an overall thermal efficiency, η, higher for CT than for PD since the influence of

Table 5
Costs calculated for the computation of LCoE at Seville location.
Source: All data were taken from [32,54,58,59].

Parabolic Dish Farm (PDF)				
			4.6 MW	20 MW
			Cost (Million USD)	
Capital costs			24.79	105.55
Equipment purchasing			16.86	73.32
	Micro Gas Turbine unit		2.555	11.12
		Turbine & Compressor	0.383	1.667
		Combustion chamber	0.255	1.111
		Power Electronics & Control System	0.894	3.890
		Recuperator	0.767	3.334
		Package	0.255	1.111
	Receiver		1.277	5.558
	Collectors field		12.35	53.71
		Land	0.054	0.236
		Parabolic Mirrors	9.902	43.072
		Wiring	0.184	0.802
		Frames & Supports	2.207	9.601
	Electrical auxiliaries		0.674	2.934
Equipment installation			3.371	14.66
Civil engineering			1.078	3.497
Natural gas substation			0.251	0.303
Project engineering			1.078	4.589
Contingencies			2.155	9.178
Decommissioning			1.078	4.589
			Cost (Million USD/year)	
Operation, maintenance and labour			3.551	13.54
Operation			3.381	10.358
	Fuel		3.377	10.343
	Water		3.217×10^{-3}	1.399×10^{-2}
Maintenance			0.517	2.193
	Direct maintenance		0.483	2.091
	Service contracts		0.034	0.102
Labour			0.653	0.994

Table 6
Main thermodynamic outputs obtained with the stated model for the three locations, two geometries and two power scales, in an annual basis. *For Dish farms brackets in E_{net} correspond to the two power levels, [4.6 MW, 20 MW].

Parameter	Ouarzazate			Seville			Salamanca		
	Central tower		Dish farm	Central tower		Dish farm	Central tower		Dish farm
	4.6 MW	20 MW		4.6 MW	20 MW		4.6 MW	20 MW	
Concentration factor	407.7	337.8	1781.0	426.3	378.1	1781.0	438.61	339.51	1781.0
Annual Solar share (f)	0.237	0.536	0.762	0.209	0.495	0.648	0.167	0.356	0.474
E_{net} (GWh/year)	40.034	185.433	[40.182, 174.793]	39.589	183.141	[39.468, 171.685]	40.497	187.484	[40.829, 177.607]
Annual overall efficiency (η)	0.358	0.341	0.235	0.357	0.340	0.234	0.373	0.369	0.246
Annual heat engine efficiency (η_H)	0.397	0.410	0.274	0.394	0.406	0.270	0.401	0.414	0.278
Annual optical efficiency (η_0)	0.648	0.625	0.909	0.654	0.605	0.909	0.659	0.607	0.909
Annual solar efficiency (η_S)	0.618	0.541	0.883	0.615	0.523	0.880	0.581	0.509	0.868
Specific fuel consumption (kg/MWh)	186.1	158.0	210.1	190.0	162.4	226.8	192.44	176.1	245.6
Specific CO_2 emissions (kg/MWh)	460.4	390.1	520.0	469.6	401.8	561.3	476.2	435.8	607.8

heat engine efficiency is bigger than that of solar efficiency (see the different role played by subsystems efficiencies in overall efficiency, Eq. (10)). The higher the power, the lower the values of achieved overall thermal efficiency for CT. Moreover, annual produced energy is larger in Salamanca because of its higher overall efficiency records, associated (as mentioned before) with better heat engines efficiencies because of lower average ambient temperatures.

From the viewpoint of the specific fuel consumption, CT 20 MW system would be a better choice, reaching minimum values of 158 kg/MWh, in the case of Ouarzazate. For Seville and Salamanca, greater natural gas consumptions are expected for producing each MWh. The correlation between fuel consumption and greenhouse emissions allows to foresee a similar behaviour for both variables. Thus, lower values of the specific CO_2 emissions are achieved for 20 MW CT layout than for the other configurations and for Ouarzazate than for the other locations.

5. Results for thermo-economic indicators

Bankability of different configurations, power scales and locations is tested through the analysis of key economic indicators, as defined in Section 2.4.

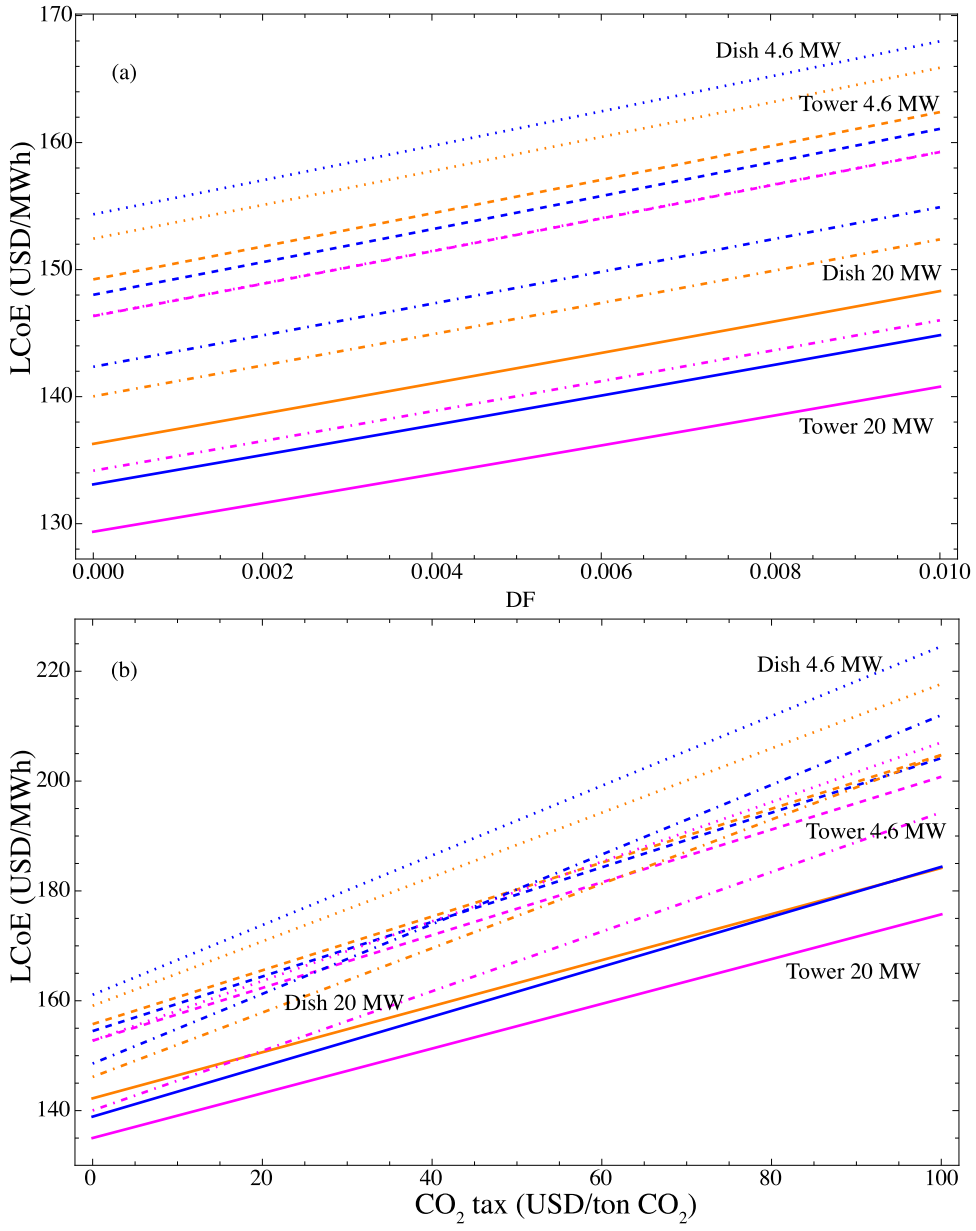

Fig. 8. Evolution of LCoE with: (a) Degradation Factor (DF) and (b) CO_2 tax. Magenta refers to Ouarzazate, orange to Seville and blue to Salamanca. Solid lines correspond to 20 MW CT system, dashed lines to 4.6 MW CT, dashed–dotted lines to 20 MW PD, and dotted ones to 4.6 MW PD.

5.1. Specific Plant Investment (SPI)

The total investment, with respect to its nominal power output, required to build a parabolic dish farm is always lower than that needed for a central tower in the three locations as well as at the two power scales (see Table 7). Differences are about 17%–19%. Variations among power scale for PD are not significant. On the other hand, for CT, location influence is shown on Ouarzazate lower values, but differences are small. It can be highlighted that 20 MW system is always related to a smaller SPI, with the only exception of Seville CT system. This exception is associated with the higher number of heliostats assumed for that configuration (see Table 1).

The SPI of those facilities is put into context in Fig. 6, where values for other kind of installations are also shown, divided into conventional, other renewable and CSP systems. Lowest values are achieved by the new version of conventional power technologies as Open Cycle Gas Turbines (OCGT), AeroDerivative Gas Turbines (ADGT) and Combined Cycle Gas Turbines (CCGT) (see Fig. 6(a)). Recent PV systems reached very low SPI too, around 900 USD/kW. A clear reduction of SPI with years is depicted for PV (see Fig. 6(b)). On the other hand, Parabolic Troughs and our CT and PD simulations still lead to high SPI. In the same line, solar central tower actual plants are associated with the highest SPIs.

Table 7
Specific Plant Investment (SPI) for the three locations, two geometries and two power scales.

SPI (USD/kW)	Central tower		Dish farm	
	4.6 MW	20 MW	4.6 MW	20 MW
Ouarzazate	6321.65	6189.50	5388.91	5275.00
Seville	6382.29	6498.99	5388.89	5274.99
Salamanca	6414.63	6210.68	5388.92	5275.01

Table 8
Levelized Cost of Electricity (LCoE) for the three locations, two geometries and two power scales.

LCoE (USD/MWh)	Central tower		Dish farm	
	4.6 MW	20 MW	4.6 MW	20 MW
Ouarzazate	[152.732,185.946]	[135.014,162.896]	[152.759,189.131]	[140.031,176.403]
Seville	[155.747,189.692]	[142.235,171.224]	[159.096,198.323]	[146.138,185.365]
Salamanca	[154.482,188.839]	[138.906,169.634]	[161.094,203.504]	[148.568,190.978]

5.2. Levelized Cost of Electricity (LCoE)

The same configurations are analysed based on Levelized Cost of Electricity (see Table 8 and Fig. 7). Uncertainty on natural gas prices and land costs leads to a range of LCoE values (see Section 3.3). It is clear that Ouarzazate stands out thanks to its low LCoEs. In that way, 20 MW CT at Ouarzazate shows the lowest LCoE, with values comprised between 135 USD/MWh and 163 USD/MWh. Among power scales, 20 MW system is always the preferred option with respect to LCoE. And, looking at CSP technologies, central towers display lower values than dish farms.

Fig. 8 is depicted for tracking the evolution of LCoE with degradation factor (DF) (see Fig. 8(a) and Eq. (16)) and with CO_2 tax (see Fig. 8(b)). It is clear that an increase of the degradation factor, and so an increase of the lost energy, implies a rise of LCoE. Results of Table 8 and Fig. 7 are calculated for a DF of 0.5%. Hence, in Fig. 8(a), the same tends than for a DF of 0.5% are kept and visualized by parallel lines. However, for the CO_2 tax evolution, lines intersect each other, which means that emissions tax behaviour is different for each layout. In the case of the 20 MW tower, with no taxes, better LCoE corresponds to Salamanca than to Seville; but for very high emissions taxes, this behaviour is reversed. As expected, the higher the CO_2 tax, the higher the LCoE.

Additionally, Fig. 9 shows the situation of simulated plants compared with other technologies. It can be highlighted that, in general, PV studies show lower LCoE values than CSP real installations, the same as wind and geothermal plants. In this way, real central tower plants present the highest LCoE among the analysed plants (see Fig. 9(c)). On the other hand, in general, simulated thermosolar systems in this work are associated with higher cost per MWh than conventional plants (see Fig. 9(a)) and other renewable facilities (see Fig. 9(b)). As a consequence, simulated LCoE agree with real CSP plants and literature data, although they are still larger than other energy generation plants. Therefore, a significant decrease of LCoE is still needed in order to make those plants bankable.

5.3. Net Present Value (NPV) and cashflows

Next, the evolution of Net Present Value (NPV) with Power Purchase Agreement price (PPA) is analysed via Fig. 10. Numerical values for both power scales are so big that two different plots are required. The intersection of NPV lines with the x axis occurs for a PPA equal to LCoE. For the 4.6 MW system, both Tower and Dish show nearly the same quantitative and qualitative performance at Ouarzazate location.

Breakdown of NPV can be better understood by means of positive and negative cashflows diagrams during power plant lifetime. As a sample, cashflows for the 20 MW system at Ouarzazate, both (a) for Central Tower and (b) for Parabolic Dish farm, are drawn at Fig. 11, based on [32]. A PPA price of 190 USD/MWh is assumed for the calculation since it is the minimum price at which all configurations are bankable. In both cases, the first two years are dedicated to the construction of the solar power plant, so a negative cashflow related to the investment cost can be visualized each year. Note that it is supposed that investment is equally divided each year. After construction, the operation period shows as positive cashflow the income from the electric energy sale, which decreases each year due to the energy degradation factor. Negative cashflows are related to operation, maintenance, labour and insurance. Finally, last two years are devoted to the decommissioning of the plant, which is reflected on a negative cashflow. Comparing between the two configurations, it is clear that investment costs are larger for the tower plant, although revenues are also higher due to its larger generated energy. Moreover, operation costs are also lower for towers than for dish farms, mainly due to fuel costs.

Table 9
Benefit to Cost Ratio (BCR), Internal Rate of Return (IRR) and Discounted Payback Period (DPP) for the three locations, two geometries and two power scales.

PPA = 190 USD/MWh				
BCR	Central tower		Dish farm	
	4.6 MW	20 MW	4.6 MW	20 MW
Ouarzazate	1.535	1.791	1.631	1.863
Seville	1.482	1.646	1.513	1.744
Salamanca	1.509	1.740	1.497	1.728
IRR (%)	Central tower		Dish farm	
	4.6 MW	20 MW	4.6 MW	20 MW
Ouarzazate	12.570	14.903	13.503	15.616
Seville	12.057	13.581	12.403	14.550
Salamanca	12.316	14.456	12.254	14.410
DPP (years)	Central tower		Dish farm	
	4.6 MW	20 MW	4.6 MW	20 MW
Ouarzazate	11.00	9.05	10.00	8.75
Seville	12.00	10.00	11.00	9.05
Salamanca	11.00	9.05	11.00	9.05

5.4. Benefit to Cost Ratio (BCR), Internal Rate of Return (IRR) and Discounted Payback Period (DPP)

Keeping a PPA of 190 USD/MWh, other economic indicators are evaluated and gathered at Table 9. Benefit to Cost Ratio is always higher than 1 since a sufficiently high PPA is assumed. The higher the BCR, the more profitable the power plant is. Accordingly, 20 MW system is always more profitable than 4.6 MW one. Parabolic dish farm constitutes a more interesting facility from BCR viewpoint than CT for Ouarzazate and Seville, but not for Salamanca. Thus, the same behaviour is found for the Internal Rate of Return (IRR). A higher IRR is achieved from PD than for CT at Ouarzazate and Seville, but not at Salamanca. Maximum IRR (15.6 %) is reached by 20 MW PD at Ouarzazate. This configuration shows also maximum BCR (1.86) and minimum Discounted Payback Period (DPP) of 8.75 years. 4.6 MW system needs more time to recover the initial investment than 20 MW one.

5.5. Required area analysis

Last key indicator takes into account the amount of land area that is needed for producing a MWh of energy. Table 10 allows to conclude than required specific land area for central towers is more than twice the area needed for dish farms. As solar field configuration is the same for all the analysed cases of parabolic farms, then the same specific area of 1.6 ha/MWh is required. For CT installations, 20 MW system requires more surface due to the undersized design of 4.6 MW solar field. Additionally, less land is employed in Ouarzazate than in the other sites.

In order to contextualize those values, a comparison with some of the biggest photovoltaic facilities in Spain [61] and with some real solar

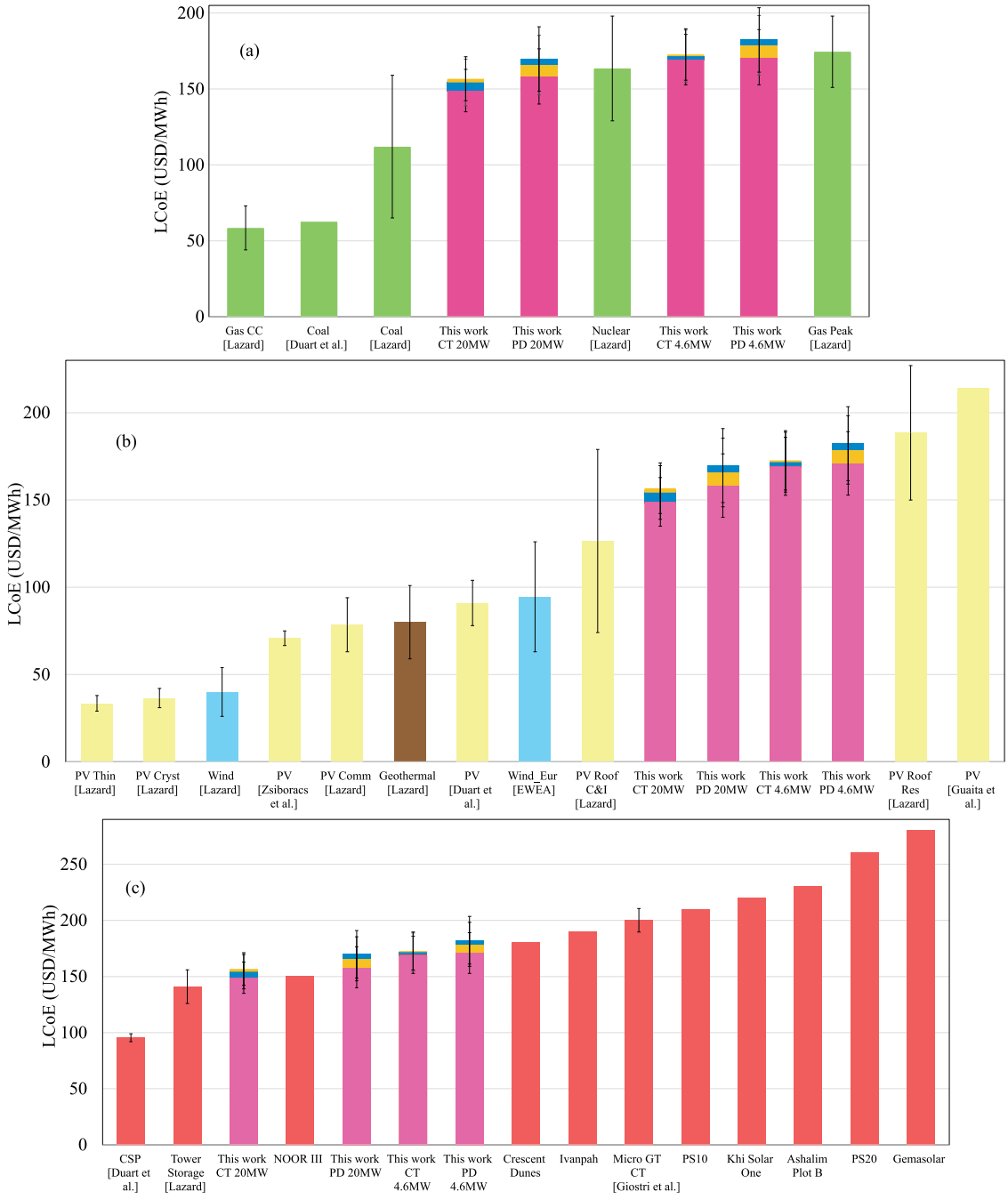

Fig. 9. Levelized Cost of Electricity (LCoE) in the context of other type of power facilities and system simulations: (a) conventional plants, (b) other renewable installations and (c) CSP projects. Magenta, orange and blue bars are associated with simulations at Ouarzazate, Seville and Salamanca locations, respectively. Cyan bars refer to wind energy, yellow ones to PV installations, brown ones to geothermal systems, red ones to other CSP systems and green bars correspond to other conventional power facilities values found in literature [47,48,50,51,60]. CC refers to Combined Cycle.

Table 10
Required specific land area for the three locations, two geometries and two power scales.

Area (ha/MWh)	Central tower		Dish farm
	4.6 MW	20 MW	
Ouarzazate	3.113	4.094	
Seville	3.260	4.535	1.589
Salamanca	3.404	4.139	

central tower installations is performed at Fig. 12. It can be highlighted that area of dish farms is low compared with PV systems and with real CT plants. On the other side, towers are associated with higher specific areas than PV, although in the order of those from real tower installations.

6. Summary and conclusions

In this work, a model for a hybrid Brayton power unit linked to CSP systems is applied to a central tower plant and also to a parabolic dish farm. In this way, the same concept is assumed for the power unit, but integrating it into two different types of solar collectors. The model for the power unit is completed with submodels for all other plant subsystems (solar collector and receiver, combustion chamber for

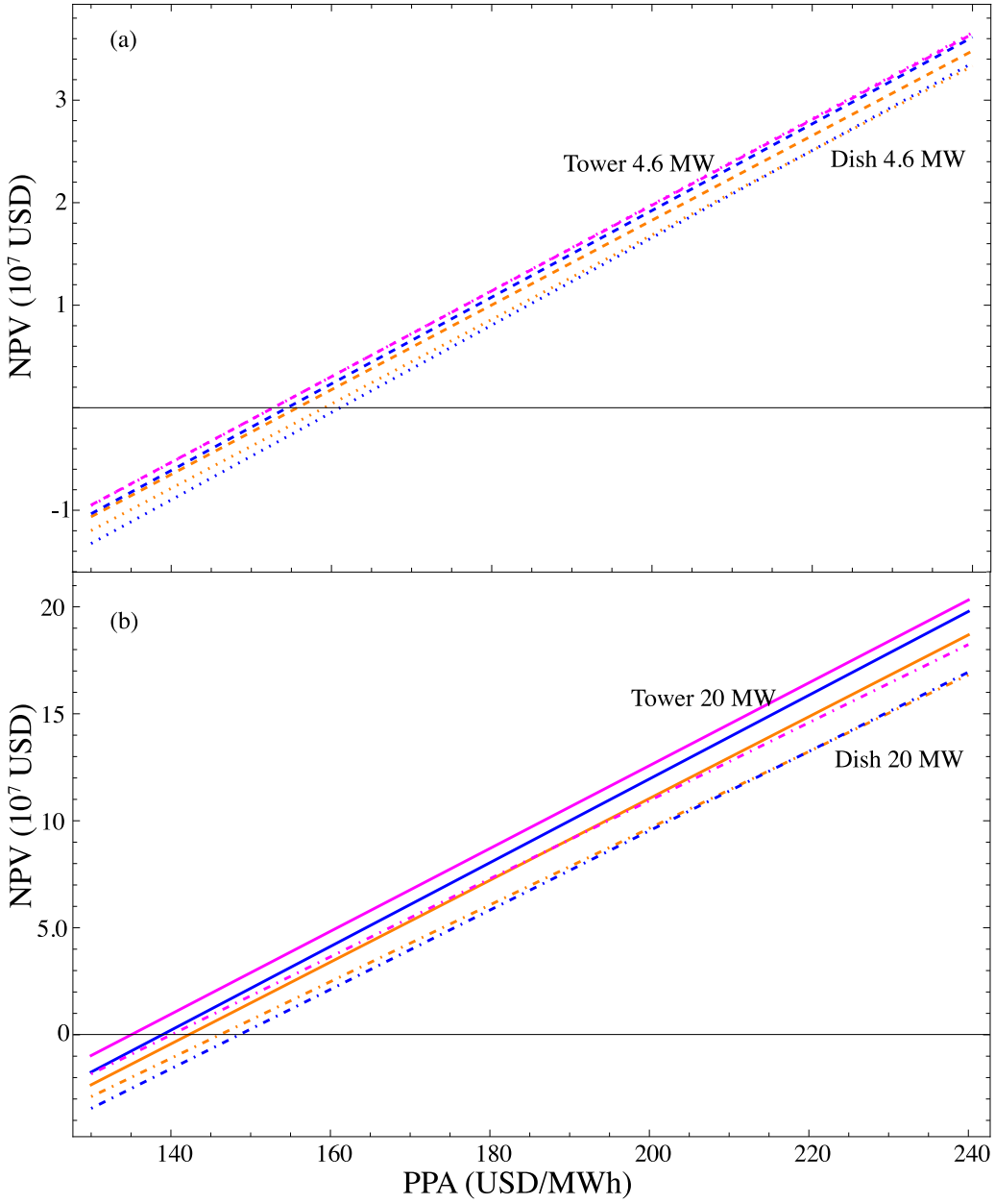

Fig. 10. Evolution of Net Present Value (NPV) with Power Purchase Agreement price (PPA) for (a) 4.6 MW and for (b) 20 MW systems. Magenta refers to Ouarzazate, orange to Seville and blue to Salamanca. Solid lines correspond to 20 MW CT system, dashed lines to 4.6 MW CT, dashed-dotted lines to 20 MW PD, and dotted ones to 4.6 MW PD.

hybridization and heat exchangers) thus, allowing to predict realistic thermodynamic and thermo-economic records. Therefore, it constitutes an integral and comprehensible model.

This model has been applied to two power levels (4.6 MW and 20 MW) in order to test scalability issues in this kind of plants. Furthermore, plant performance has been evaluated at three different locations sited on a south–north line from Ouarzazate (Morocco) to Salamanca (Spain), passing by Seville (Spain), covering a wide latitude interval. Those sites present quite different solar and meteorological conditions whose influence on the plant behaviour is analysed. With the aim of carrying out this test, real solar and meteorological data have been employed. Outcomes are processed to get annual averages in the estimation of key thermo-economic indicators. Regarding costs assessment, accurate and realistic correlations are considered.

In a first analysis, thermodynamic records have been evaluated on an annual basis. A first conclusion is that overall efficiencies of these high temperature plants (upper temperatures reach about 1100–1400 K), for whichever type of solar concentrators, are remarkably high, between 0.24 and 0.37 at real conditions (yearly averaged). A significant outcome is that parabolic dish farm behaviour is independent of power scale, except for net energy. Larger solar share records are found, as expected, for locations with higher solar irradiation. Nevertheless, a key conclusion is that locations with low average ambient temperature and medium–high solar irradiance can give good results in overall efficiency, with no dependence on power scale nor solar collector type. The particular case of 4.6 MW central tower system is inspired by SOLUGAS Project, whose original undersized solar field has a clear effect on plant performance: small solar share and high specific fuel consumption and, so, high specific CO_2 emissions.

The second part of this study has been devoted to analyse the thermo-economic estimations through some key indicators. In this line, Specific Plant Investment of simulated systems was compared

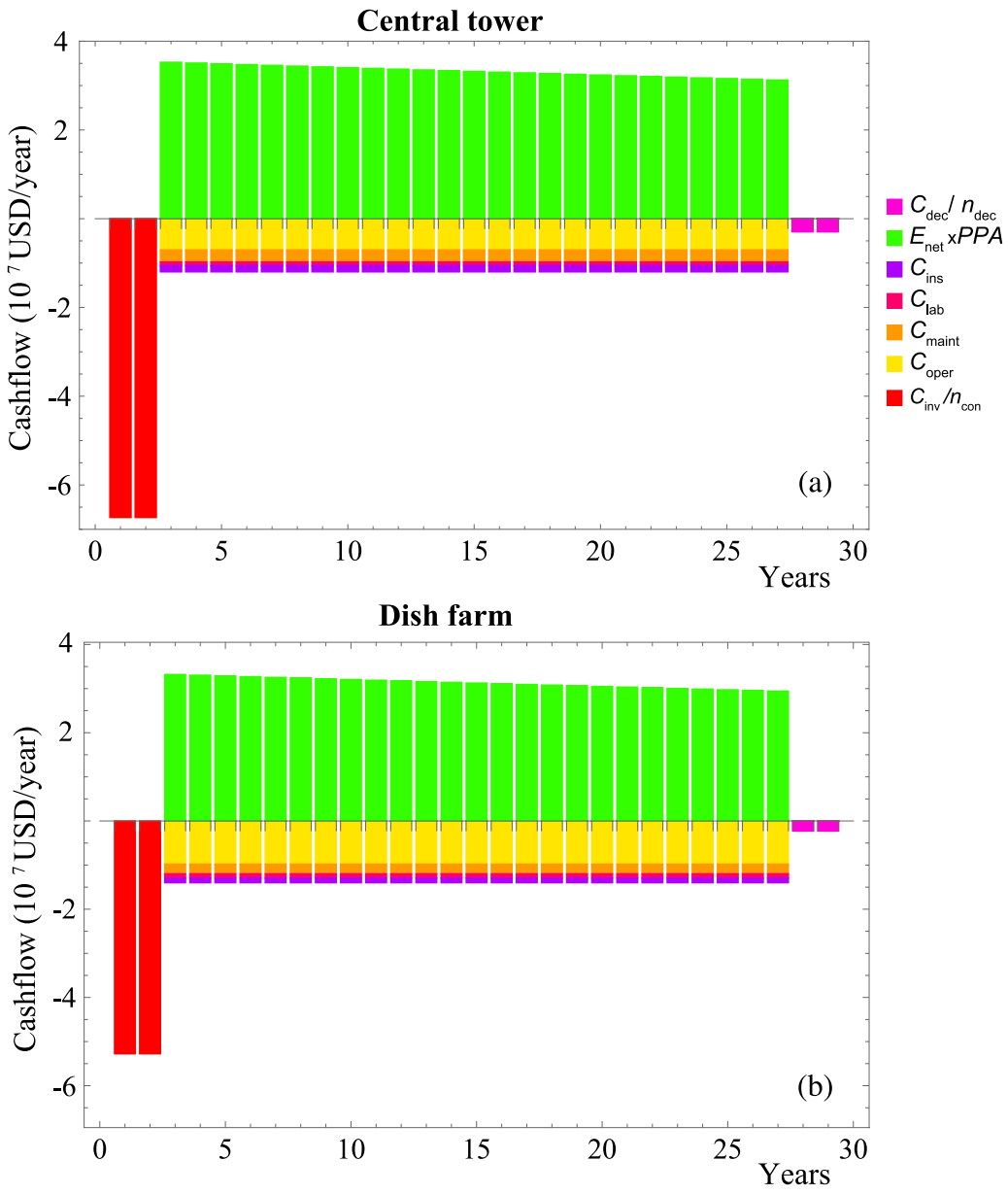

Fig. 11. Cashflows for Ouarzazate 20 MW. (a) Central tower and (b) parabolic dish farm configurations. PPA was fixed at 190 USD/MWh.

against conventional, other renewable and other Concentrated Solar Power plants. SPI is similar or even lower than that of real solar tower installations, which employ Rankine cycles as heat engines and work at medium temperatures. Among analysed layouts, LCoE is minimum for 20 MW solar tower system at Ouarzazate location, reaching [135–163] USD/MWh. This range has been computed for reflecting uncertainty of natural gas and land prices. In addition, the higher the power scale, the lower the LCoE. It has also been noted that central tower geometry is related to smaller LCoE values than parabolic dish farms. Ouarzazate stands out as the best location concerning LCoE. Moreover, the evolution of LCoE with Degradation Factor and with CO_2 tax has been assessed, showing linear behaviours in all cases. Corresponding slopes have also been computed. As for SPI, simulated LCoEs have been compared with other power technologies demonstrating that they are competitive against other conventional plants, being also lower than most of other CSP considered installations. On the opposite, simulated values are higher than wind and most PV analysed plants.

Furthermore, Power Purchase Agreement price influence on Net Present Value has been analysed and cashflows estimated. It can be stressed that initial investment in central towers is higher than in parabolic dishes, but operation costs are lower. Finally, specific required area analysis showed a quite smaller necessity of land for dish farms than for central towers, which is even lower than that of most novel PV plants, for instance, in Spain. On the other hand, central tower plants display higher land requirements, which increase with plant size in relative terms as shown in Table 10. The latter happens because of the particularly undersized SOLUGAS solar field. Therefore, in order to extrapolate this behaviour to a generic plant, the same level of hybridization should be considered at both power scales.

On the whole, both thermodynamic and thermo-economic estimations obtained from this study make this technology promising. Nevertheless, LCoE and SPI still need to be decreased for fully commercial deployment. In particular, a reduction on equipment purchasing and operation costs is crucial. As future work, high temperature storage should be implemented in the simulations and, thus, probably LCoE will decrease because operation cost would not include fuel line item.

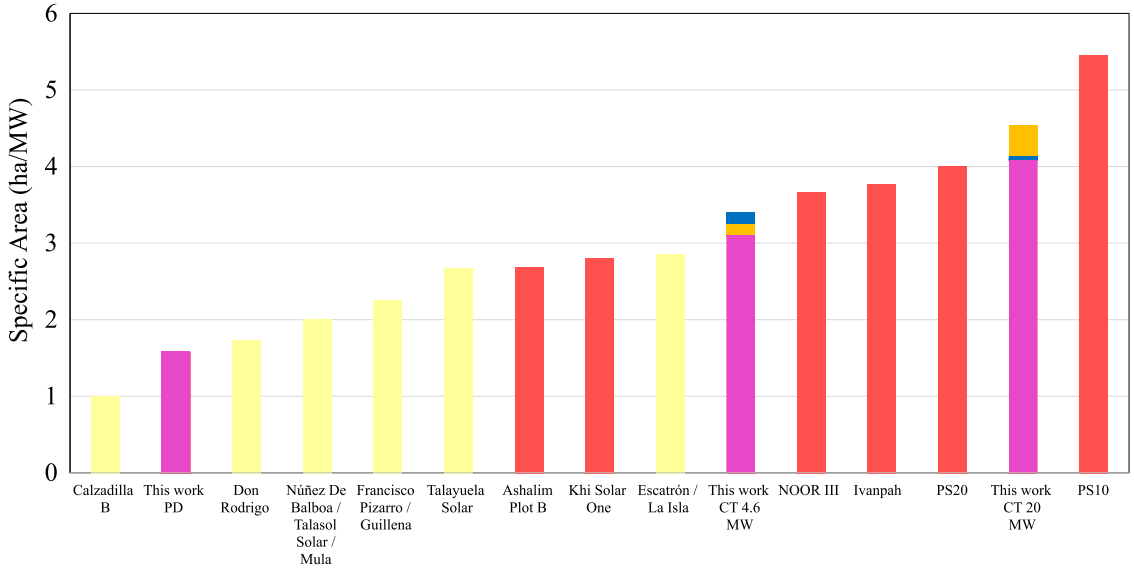

Fig. 12. Required specific area in the context of other CSP plants of some of the biggest PV facilities in Spain [61]. Yellow bars correspond to PV installations, red ones to Solar Central Tower systems, and magenta, orange and blue bars are associated with both Parabolic Dish and Central Tower simulated systems, at Ouarzazate, Seville and Salamanca locations, respectively.

Moreover, this will lead to the development of fully renewable plants with zero emissions if natural gas hybridization is substituted by energy storage.

CRediT authorship contribution statement

J. García-Ferrero: Software, Investigation, Review and editing, Visualization. **R.P. Merchán:** Software, Investigation, Writing – original draft. **M.J. Santos:** Conceptualization, Validation, Review and editing. **A. Medina:** Conceptualization, Validation, Investigation, Writing – original draft. **A. Calvo Hernández:** Review and editing, Supervision.

Declaration of competing interest

The authors declare that they have no known competing financial interests or personal relationships that could have appeared to influence the work reported in this paper.

Data availability

Data will be made available on request.

Acknowledgements

The authors thank financial support from Universidad de Salamanca through *Programa I: Programa de Financiación de Grupos de Investigación* and Fundación General Universidad de Salamanca, PC_TCUE18-20P_010. R.P. Merchán acknowledges postdoctoral contracts from Universidad de Salamanca and Banco de Santander. All authors read and agreed to the published version of the manuscript.

References

[1] Technology Roadmaps. Concentrating solar power. Tech. rep., International Energy Agency IEA; 2010, http://dx.doi.org/10.1787/9789264088139-en.
[2] van der Hoeven M. Technology roadmap solar thermal electricity. Tech. rep. 52, International Energy Agency (IEA); 2014, URL https://webstore.iea.org/technology-roadmap-solar-thermal-electricity-2014.
[3] Behar O, Khellaf A, Mohammedi K. A review of studies on central receiver solar thermal power plants. Renew Sust Energy Rev 2013;23:12–39.
[4] Achkari O, El Fadar A. Latest developments on TES and CSP technologies-energy and environmental issues, applications and research trends. Appl Therm Eng 2020;167:114806.
[5] Gauché P, Rudman J, Mabaso M, Landman W, von Backström T, Brent A. System value and progress of CSP. Sol Energy 2017;152:106–39. http://dx.doi.org/10.1016/j.solener.2017.03.072.
[6] Dunham M, Iverson B. High-efficiency thermodynamic power cycles for concentrated solar power systems. Renew Sustain Energy Rev 2014;30:758–70.
[7] Palacios A, Barreneche C, Navarro M, Ding Y. Thermal energy storage technologies for concentrated solar power-A review from a materials perspective. Renew Energy 2020;156:1244–65. http://dx.doi.org/10.1016/j.renene.2019.10.127.
[8] Pramanik S, Ravikrishna RV. A review of concentrated solar power hybrid technologies. Appl Therm Eng 2017;127:602–37.
[9] Merchán RP, Santos MJ, Medina A, Calvo Hernández A. High temperature central tower plants for concentrated solar power: 2021 overview. Renew Sustain Energy Rev 2022;155:111828. http://dx.doi.org/10.1016/j.rser.2021.111828.
[10] He YL, Qiu Y, Wang K, Yuan F, Wang WQ, Li MJ, et al. Perspective of concentrating solar power. Energy 2020;198:117373. http://dx.doi.org/10.1016/j.energy.2020.117373.
[11] Santos MJ, Miguel-Barbero C, Merchán RP, Medina A, Calvo Hernández A. Roads to improve the performance of hybrid thermosolar gas turbine power plants: Working fluids and multi-stage configurations. Energy Convers Manage 2018;165:578–92.
[12] Khatoon S, Kim M-H. Preliminary design and assessment of concentrated solar power plant usingsupercritical carbon dioxide Brayton cycles. Energy Convers Manage 2022;252:115066. http://dx.doi.org/10.1016/j.enconman.2021.115066.
[13] Chen R, Romero M, González-Aguilar J, Rovense F, Rao Z, Liao S. Optical and thermal integration analysis of supercritical co_2 brayton cycles with a particle-based solar thermal plant based on annualperformance. Renew Energy 2022;189:164–79. http://dx.doi.org/10.1016/j.renene.2022.02.059.
[14] Sedighi M, Vasquez Padilla R, Taylor R, Lake M, Izadgoshasb I, Rose A. High-temperature, point-focus, pressurised gas-phase solar receivers: A comprehensive review. Energy Convers Manage 2019;185:678–717. http://dx.doi.org/10.1016/j.enconman.2019.02.020.
[15] Merchán RP, Santos MJ, Heras I, Gonzalez-Ayala J, Medina A, Calvo Hernández A. On-design pre-optimization and off-design analysis of hybrid brayton thermosolar tower power plants for different fluids and plant configurations. Renew Sustain Energy Rev 2020;119:109590. http://dx.doi.org/10.1016/j.rser.2019.109590.
[16] Merchán RP, Santos MJ, Medina A, Calvo Hernández A. On- and off-design thermodynamic analysis of a hybrid polar solar thermal tower power plant. Int J Energy Res 2021;45:1789–805. http://dx.doi.org/10.1002/er.5854.
[17] Merchán RP, Santos MJ, García-Ferrero J, Medina A, Calvo Hernández A. Thermo-economic and sensitivity analysis of a central tower hybrid brayton solar power plant. Appl Therm Eng 2021;186:116454. http://dx.doi.org/10.1016/j.applthermaleng.2020.116454.
[18] García-Ferrero J, Heras I, Santos MJ, Merchán RP, Medina A, González A, et al. Thermodynamic and cost analysis of a solar dish power plant in Spain hybridized with a micro-gas turbine. Energies.
[19] WolframAlpha. Mathematica. URL https://www.wolfram.com/mathematica/.
[20] Barberena J, Mutuberria Larrayoz A, Sánchez M, Bernardos A. State-of-the-art of heliostat field layout algorithms and their comparison. Energy Proc 2016;93:31–8.

[21] Jafrancesco D, Cardoso J, Mutuberria A, Leonardi E, Les I, Sansoni P, et al. Optical simulation of a central receiver system: Comparison of different software tools. Renew Sustain Energy Rev 2018;94:792–803.

[22] Collado F. Preliminary design of surrounding heliostat fields. Renew Energy 2009;34:1359–63.

[23] Collado F, Guallar J. Campo: Generation of regular heliostat fields. Renew Energy 2012;46:49–59.

[24] Schmitz M, Schwarzbozl P, Buck R, Pitz-Paal R. Assessment of the potential improvement due to multiple apertures in central receiver systems with secondary concentrators. Sol Energy 2006;80:111–20. http://dx.doi.org/10.1016/j.solener.2005.02.012.

[25] Collado F, Guallar J. A review of optimized design layouts for solar power tower plants with campo code. Renew Sustain Energy Rev 2013;20:142–54.

[26] Stine W, Geyer M. Power from the sun. 2001, URL http://www.powerfromthesun.net/book.html.

[27] Noone CJ, Torilhon M, Mitsos A. Heliostat field optimization: A new computationally efficient model and biomimetic layout. Sol Energy 2012;86:792–803.

[28] Blanco MJ, Amieva JM, Mancillas A. The tonatiuh software development project: An open source approach to the simulation of solar concentrating systems. Comput Inf Eng 2005;2005:157–64.

[29] Duffie J, Beckman W. Solar engineering of thermal processes. Hoboken, New Jersey: John Wiley and Sons; 2006, URL https://onlinelibrary.wiley.com/doi/pdf/10.1002/9781118671603.

[30] Olivenza-León D, Medina A, Calvo Hernández A. Thermodynamic modeling of a hybrid solar gas-turbine power plant. Energy Convers Manage 2015;93:435–47.

[31] Merchán RP, Santos MJ, Reyes-Ramírez I, Medina A, Calvo Hernández A. Modeling hybrid solar gas-turbine power plants: Thermodynamic projection of annual performance and emissions. Energy Convers Manage 2017;134:314–26. http://dx.doi.org/10.1016/j.enconman.2016.12.044.

[32] Spelling J. Hybrid solar gas-turbine power plants [Ph.D. thesis], Stockholm, Sweden: KTH Royal Institute of Technology, Department of Energy Technology; 2013.

[33] Abdelhady S. Performance and cost evaluation of solar dish power plant: Sensitivity analysis of levelized cost of electricity (LCOE) and net present value (NPV). Renew Energy 2021;168:332–42. http://dx.doi.org/10.1016/j.renene.2020.12.074.

[34] Copernicus atmosphere monitoring service (ECMWF). 2018, URL http://www.soda-pro.com/web-services/radiation/cams-radiation-service. [Accessed 11 April 2021].

[35] SOLARGIS solar resource maps and GIS data. URL https://solargis.com/es/maps-and-gis-data/download/spain.

[36] Investopedia. URL https://www.investopedia.com.

[37] Korzynietz R, Brioso J, del Río A, Quero M, Gallas M, Uhlig R, et al. Solugas-comprehensive analysis of the solar hybrid Brayton plant. Sol Energy 2016;135:578–89.

[38] Burgaleta S, Ramírez D. Gemasolar, the first tower thermosolar commercial plant with molten salt storage. In: Proceedings of solarPACES. Granada, Spain; 2011.

[39] Solar turbines-caterpillar. 2021, URL https://mysolar.cat.com/cda/files/126873/7/dsm50pg.pdf. [Accessed 10 September 2021].

[40] Solar turbines-caterpillar. 2021, URL https://www.solarturbines.com. [Accessed 10 September 2021].

[41] Semprini S, Sánchez D, De Pascale A. Performance analysis of a micro gas turbine and solar dish integrated system under different solar-only and hybrid operating conditions. Sol Energy 2016;132:279–93.

[42] Capstone Turbine Corporation, Capstone C30 Turbine. URL https://www.pureworldenergy.com/media/filer_public/d8/d9/d8d9f29a-b680-4ccc-bf62-a8cf59f3a435/c30_hpng_331140a.pdf, https://www.capstoneturbine.com/products/c30.

[43] Giostri A, Macchi E. An advanced solution to boost sun-to-electricity efficiency of parabolic dish. Sol Energy 2016;139:337–54.

[44] Modern era retrospective analysis for research and applications (MERRA). 2021, URL http://www.soda-pro.com/web-services/meteo-data/merra. [Accessed 15 February 2021].

[45] Nabe C, O'Malley M, Bömer J, Broad D. The Irish 'all island grid study' - methodological approach and outcomes. In: 2009 Power systems conference and exposition. IEEE.

[46] Zsiboracs H, Baranyai N. An economic analysis of the shading effects of transmission lines on photovoltaic power plant investment decisions: A case study. Sensors 2021;21:4973. http://dx.doi.org/10.3390/s21154973.

[47] Krohn S, Morthorst P, Awerbuch S. The economics of wind energy. 2009.

[48] Guaita-Pradas I, Soucase B. Endorse of renewable energy plants, still an alternative investment in Spain? SOP Trans Econ Res 2014;1(2):1–9.

[49] Henchoz S, Buchter F, Favrat D, Morandin M, Mercangöz M. Thermoeconomic analysis of a solar enhanced energy storage concept based onthermodynamic cycles. Energy 2012;45:358–65. http://dx.doi.org/10.1016/j.energy.2012.02.010.

[50] Hernández-Moro J, Martínez-Duart JM. Analytical model for solar PV and CSP electricity costs present LCOE values and their future evolution. Renew Sustain Energy Rev 2013;20:119–32.

[51] Giostri A, Binotti M, Sterpos C, Lozza G. Small scale solar tower coupled with micro gas turbine. Renew Energy 2020;147:570–83.

[52] Augsburger G. Thermo-economic optimisation of large solar tower power plants [Ph.D. thesis], 2013.

[53] Mohammadi K, McGowan JG, Saghafifar M. Thermoeconomic analysis of multi-stage recuperative brayton power cycles: Part I- hybridization with a solar power tower system. Energy Convers Manage 2019;185:898–919.

[54] Swift, Marshall. Marshall & Swift valuation services. Inventory index factors. 2018, URL https://www.corelogic.com/products/marshall-swift-valuation-service.aspx.

[55] Informe de supervisión del mercado de gas natural en españa. Tech. rep. IS/DE/007/19, Comisión Nacional de los Mercados y la Competencia (CNMC), URL https://www.cnmc.es/sites/default/files/2647322.pdf.

[56] Agua del grifo: Grandes diferencias de precio. 2021, URL https://www.ocu.org/alimentacion/agua/noticias/precios-agua-grifo-2020. [Accessed 19 November 2021].

[57] El precio de la tierra sigue al alza en salamanca. 2020, URL https://lacronicadesalamanca.com/296876-el-precio-de-la-tierra-sigue-al-alza-en-salamanca-con-el-regadio-como-estrella/. [Accessed 29 November 2020].

[58] Ragnolo G. A techno-economic comparison of a micro gas-turbine and a stirling engine for solar dish application [Ph.D. thesis], Stockholm, Sweden: KTH School of Industrial Engineering and Management, Energy Technology Department; 2013.

[59] Snidvongs S. The structure and foundation design for small solar thermal dish stirling 10 kw power plant for Thailand softland and poor isolation nature. In: ASME 2005 international solar energy conference. 2005, http://dx.doi.org/10.1115/ISEC2005-76017.

[60] Levelized cost of energy and levelized cost of storage - 2020. 2020, URL https://www.lazard.com/perspective/lcoe2020.

[61] Álvarez C, Zafra M. Cuánto ocupan las megacentrales solares: Investigadores alertan del impacto del 'boom' fotovoltaico. URL https://elpais.com/clima-y-medio-ambiente/2021-01-23/cuanto-ocupan-las-megacentrales-solares-investigadores-alertan-del-impacto-del-boom-fotovoltaico.html.